TKK Dissertations 77
Espoo 2007

SELF-ASSEMBLED INDIUM PHOSPHIDE NANOWIRES

Doctoral Dissertation

Marco Mattila

Helsinki University of Technology
Department of Electrical and Communications Engineering
Micro and Nanosciences Laboratory

TKK Dissertations 77
Espoo 2007

SELF-ASSEMBLED INDIUM PHOSPHIDE NANOWIRES

Doctoral Dissertation

Marco Mattila

Dissertation for the degree of Doctor of Science in Technology to be presented with due permission of the Department of Electrical and Communications Engineering for public examination and debate in Auditorium AS1 at Helsinki University of Technology (Espoo, Finland) on the 15th of June, 2007, at 12 noon.

Helsinki University of Technology
Department of Electrical and Communications Engineering
Micro and Nanosciences Laboratory

Teknillinen korkeakoulu
Sähkö- ja tietoliikennetekniikan osasto
Mikro- ja nanotekniikan laboratorio

Distribution:
Helsinki University of Technology
Department of Electrical and Communications Engineering
Micro and Nanosciences Laboratory
P.O. Box 3500
FI - 02015 TKK
FINLAND
URL: http://www.micronova.fi/units/ntg/
Tel. +358-9-4511
Fax +358-9-451 3128
E-mail: marco.mattila@tkk.fi

© 2007 Marco Mattila

ISBN 978-951-22-8812-0
ISBN 978-951-22-8813-7 (PDF)
ISSN 1795-2239
ISSN 1795-4584 (PDF)
URL: http://lib.tkk.fi/Diss/2007/isbn9789512288137/

TKK-DISS-2311

Multiprint Oy
Espoo 2007

HELSINKI UNIVERSITY OF TECHNOLOGY P. O. BOX 1000, FI-02015 TKK http://www.tkk.fi	ABSTRACT OF DOCTORAL DISSERTATION
Author Marco Mattila	
Name of the dissertation Self-assembled indium phosphide nanowires	
Date of manuscript April 13th, 2007	Date of the dissertation June 15th, 2007
Article dissertation (summary + original articles)	Number of pages 56 + 32
Department Department of Electrical and Communications Engineering Laboratory Micro and Nanosciences Laboratory Field of research Nanotechnology Opponent Professor Knut Deppert Supervisor Professor Harri Lipsanen	

Abstract

This thesis deals with the self-assembled vapor-liquid-solid (VLS) growth and properties of InP nanowires, concentrating mainly on the novel catalyst-free growth of InP nanowires using *in situ* deposited indium droplets as seeds in metalorganic vapor phase epitaxy. The fabricated nanowires were characterized using scanning and transmission electron microscopy and continous-wave and time-resolved photoluminescence spectroscopy. All demonstrated nanowires have potential applications in nanophotonics and electronics.

Epitaxial catalyst-free VLS growth of InP nanowires on (111)B InP substrates was demonstrated. The resulting distribution of vertical, freely standing nanowires is fairly homogeneous at an areal density of 10^9–10^{10} cm^{-2}. An indium droplet without phosphorus at the nanowire tip indicates VLS growth. The average nanowire diameter (20–40 nm) and length (250–550 nm) as well as tapering can be controlled by adjusting the growth parameters. The same growth method was also shown to work to some extent for nanowire growth on silicon. The growth of ternary InAsP nanowires was briefly examined.

The growth direction investigations included nanowire fabrication also on (111)A, (110), and (001) InP substrates. Electron microscopy analyses showed that the nanowire axis is parallel to $\langle 111 \rangle$B on all studied substrate orientations. The crystalline structure is mainly zinc-blende with a large number of twin stacking faults per unit length.

Homoepitaxial catalyst-free-grown InP nanowires exhibit room temperature photoluminescence at 1.38 eV, blue shifted by about 30 meV from the band gap energy of cubic InP. Due to the large surface-to-volume ratio of the nanowires, the internal quantum efficiency for radiative carrier recombination is highly sensitive to surface conditions. The nanowires were passivated by hydrofluoric acid treatment which results in a 100-fold increase in the photoluminescence intensity, enabling the measurement of carrier recombination dynamics by means of time-resolved photoluminescence measurements. Double-exponential decay was observed, suggesting surface-related recombination processes. Finally, growth of InP nanowires using gold nanoparticle catalysts was studied. The photoluminescence and x-ray diffraction results suggest that the nanowires can crystallize in both cubic and hexagonal phases, depending on the growth temperature.

Keywords Nanowire, self-assembled, InP, catalyst-free, vapor-liquid-solid, VLS, MOVPE	
ISBN (printed) 978-951-22-8812-0	ISSN (printed) 1795-2239
ISBN (electronic) 978-951-22-8813-7	ISSN (electronic) 1795-4584
Publisher TKK Micro and Nanosciences Laboratory	
Print distribution TKK Micro and Nanosciences Laboratory	
The dissertation can be read at http://lib.tkk.fi/Diss/2007/isbn9789512288137/	

TEKNILLINEN KORKEAKOULU PL 1000, 02015 TKK http://www.tkk.fi	VÄITÖSKIRJAN TIIVISTELMÄ

Tekijä Marco Mattila

Väitöskirjan nimi

Self-assembled indium phosphide nanowires

Käsikirjoituksen jättämispäivämäärä 13.4.2007	Väitöstilaisuuden ajankohta 15.6.2007
Yhdistelmäväitöskirja (yhteenveto + erillisartikkelit)	Sivumäärä 56 + 32

Osasto	Sähkö- ja tietoliikennetekniikan osasto
Laboratorio	Mikro- ja nanotekniikan laboratorio
Tutkimusala	Nanoteknologia
Vastaväittäjä	Prof. Knut Deppert
Työn valvoja	Prof. Harri Lipsanen

Tiivistelmä

Väitöskirja käsittelee InP-nanolankojen itseorganisoituvaa kasvua vapor-liquid-solid-menetelmällä (VLS). Tutkimus keskittyy uuteen katalyytittömään VLS-menetelmään, jossa alustakiteen pintaan muodostetaan indiumpisaroita organometallista kaasufaasiepitaksialaitteistoa käyttäen ilman muita prosessivaiheita. Nanolankojen karakterisointi tapahtuu pyyhkäisy- ja läpäisyelektronimikroskopian sekä jatkuvatoimisen ja ajasta riippuvan fotoluminesenssispektroskopian avulla. Tutkituilla nanolangoilla on potentiaalisia käyttökohteita nanofotoniikan ja -elektroniikan sovelluksissa.

Työssä valmistettiin epitaksiaalisia InP-nanolankoja (111)B InP -alustakiteille katalyytitöntä VLS-menetelmää käyttäen. Valmistettujen homogeenisten ja pystysuorien nanolankojen pintatiheys on 10^9–10^{10} cm^{-2}. Nanolankojen halkaisija (20–40 nm), pituus (250–550 nm) ja muoto on säädettävissä kasvatusparametrien avulla. Samalla menetelmällä valmistettiin myös In(As)P-nanolankoja piialustakiteen päälle.

Nanolankojen kasvua tutkittiin myös (111)A, (110) ja (001) InP -alustakiteille. Kasvusuunnaksi havaittiin $\langle 111 \rangle$B alustakiteen orientaatiosta riippumatta. Nanolangat kiteyvät pääosin sinkkivälkehilaan, jossa havaitaan suuri määrä pinousvirheitä.

Homoepitaksiaaliset katalyytittömällä VLS-menetelmällä valmistetut InP-nanolangat luminoivat huoneenlämpötilassa suoritetuissa fotoluminesenssimittauksissa energialla 1,38 eV, noin 30 meV kuutiollisen indiumfosfidin kiellettyä energiaväliä suuremmalla energialla. Nanolangan pinta-ala on suuri suhteessa sen tilavuuteen. Tämän takia pinnalla on suuri merkitys säteilevän rekombinaation hyötysuhteeseen. Fluorivetyhappokäsittely passivoi nanolankojen pintatilat, mikä nähtiin fotoluminesenssi-intensiteetin satakertaistumisena ja mikä mahdollisti rekombinaatiodynamiikan tutkimisen ajasta riippuvilla fotoluminesenssimittauksilla. Kaksoiseksponentiaalinen fotoluminesenssisignaalin vaimeneminen osoittaa pintatilojen edelleen vaikuttavan nanolankojen optisiin ominaisuuksiin. Työssä tutkittiin InP-nanolankojen valmistusta VLS-menetelmällä myös kultananopartikkelikatalyytein. Fotoluminesenssi- ja röntgendiffraktiotulosten perusteella nanolangat voivat kiteytyä kuutiolliseen tai heksagonaaliseen hilaan kasvatuslämpötilasta riippuen.

Asiasanat Nanolanka, itseorganisoituva, InP, katalyytitön, vapor-liquid-solid, VLS, MOVPE

ISBN (painettu)	978-951-22-8812-0	ISSN (painettu)	1795-2239
ISBN (elektroninen)	978-951-22-8813-7	ISSN (elektroninen)	1795-4584

Julkaisija TKK Mikro- ja nanotekniikan laboratorio

Painetun väitöskirjan jakelu TKK Mikro- ja nanotekniikan laboratorio

Luettavissa verkossa osoitteessa http://lib.tkk.fi/Diss/2007/isbn9789512288137/

Preface

As of early year 2000, after having wandered for the first time into the late Optoelectronics Laboratory at Helsinki University of Technology, I have been involved in various interesting fields of research pertaining to compound semiconductors and the now more or less legendary fabrication equipment thereof. For that opportunity I have to thank the past and the present laboratory executives, Professor Turkka Tuomi, Professor Harri Lipsanen, and Docent Markku Sopanen. For help in crystallizing the latest subject – nanowires – into the dissertation you – the reader – are browsing through right now, I have to thank also Doctor Teppo Hakkarainen, Doctor Mikael Mulot, Doctor Hua Jiang, and Professor Esko Kauppinen. As an added bonus, I have had the pleasure to work with the rest of the great crew of the Laboratory in several other projects.

The Graduate School of Modern Optics and Electronics, Tekniikan edistämissäätiö, Jenny and Antti Wihuri Foundation, and Emil Aaltosen Säätiö are all acknowledged for financially supporting my work.

For support and encouragement during all my studies starting from day one, I am grateful to my parents and my sister. Finally, I thank my wife Päivi for love and positive spirit.

Espoo, May 2007

Marco Mattila

Contents

Preface vii

Contents viii

List of publications ix

Author's contribution x

1 Introduction 1

2 Semiconductor nanowires 3
- 2.1 Vapor-liquid-solid growth . . . 3
- 2.2 Catalyst-free nanowire growth . . . 5
- 2.3 Other growth mechanisms . . . 8
- 2.4 Nanowire devices and applications . . . 9

3 Experimental methods 11
- 3.1 Metalorganic vapor phase epitaxy . . . 11
- 3.2 Optical characterization . . . 12
- 3.3 Electron microscopy . . . 15
- 3.4 X-ray diffraction . . . 17

4 Catalyst-free indium phosphide nanowires 18
- 4.1 Size-controlled growth on indium phosphide . . . 18
- 4.2 Nanowire growth on silicon . . . 22
- 4.3 Crystal structure of catalyst-free-grown nanowires . . . 24
- 4.4 Nanowire photoluminescence . . . 29

5 Gold-nanoparticle-catalyzed indium phosphide nanowires 34
- 5.1 Nanowire growth . . . 34
- 5.2 Photoluminescence and crystal structure . . . 35

6 Summary and outlook 37

List of publications

This thesis consists of an overview and of the following publications which are referred to in the text by their Roman numerals.

I M. Mattila, T. Hakkarainen, and H. Lipsanen, *Catalyst-free fabrication of InP and InP(N) nanowires by metal organic vapor phase epitaxy*, Journal of Crystal Growth **298** 640 (2007)

II M. Mattila, T. Hakkarainen, H. Lipsanen, H. Jiang, and E. I. Kauppinen, *Catalyst-free growth of In(As)P nanowires on silicon*, Applied Physics Letters **89** 063119 (2006)

III M. Mattila, T. Hakkarainen, H. Jiang, E. I. Kauppinen, and H. Lipsanen, *Effect of substrate orientation on the catalyst-free growth of InP nanowires*, Nanotechnology **18** 155301 (2007)

IV M. Mattila, T. Hakkarainen, H. Lipsanen, H. Jiang, and E. I. Kauppinen, *Enhanced luminescence from catalyst-free grown InP nanowires*, Applied Physics Letters **90** 033101 (2007)

V M. Mattila, T. Hakkarainen, M. Mulot, and H. Lipsanen, *Crystal-structure-dependent photoluminescence from InP nanowires*, Nanotechnology **17** 1580 (2006)

Author's contribution

Nanowire growth and characterization for publications I, II, III, and IV was done by the author. For publication V, sample fabrication and optical characterization were done by the author and T. Hakkarainen, and electron microscopy measurements were performed by the author with the assistance of M. Mulot. The transmission electron microscopy measurements and analyses for publications II, III, and IV were performed by H. Jiang. The manuscripts for all publications included in this thesis were written by the author.

1 Introduction

Attempts to build small things using ever smaller building blocks has led to the discovery of new tools and methods for manipulation of matter and fabrication of structures in the nanometer scale. Typically, fabrication of a semiconductor device consists of growing an epitaxial layer structure on a substrate and post-processing using lithography and etching. As it turns out, self-assembling methods have proven to be viable alternatives to this traditional fabrication approach. Objects offering zero-dimensional confinement for charge carriers, quantum dots, are available using, *e.g.*, self-assembled semiconductor islands. The self-assembled growth of their counterpart in one dimension, the quantum wire, was demonstrated in the early nineties based on the vapor-liquid-solid method first proposed by Wagner and Ellis over forty years ago for the growth of micrometer-sized silicon whiskers [1]. More recently, other growth methods and applications for quantum wires, and more generally, nanowires, wire-like structures with diameters smaller than 100 nm and aspect ratios greater than ∼10, have been demonstrated or proposed [2–4].

In addition to new types of devices, physics of low-dimensional structures can also be explored using semiconductor nanowires. A lot of mesoscopic phenomena have characteristic lengths in the range of 1–500 nm, such as the exciton Bohr radius, phonon and electron mean free paths, and the Debye length [2]. Nanowires and nanowire heterostructures readily allow experimental access and controllable optical and transport properties within this range, enabling single-molecule, single-electron, or single-photon operation, something that is seen as one of the goals of nanotechnology. Although nanotechnology has received a lot of hype in the media, it has received also negative publicity because of its possible negative impact on the environment and people. Production issues aside, small nanoparticles, such as nanowires, are considered toxic and can have high mobilities in the atmosphere and human body. Indeed, from a structural point of view, nanowires are very similar to asbestos fibers known to cause serious diseases in humans. However, these concerns should not stand in the way of the development of devices based on possibly harmful entities, as long as suitable precautions are taken to prevent their release outside the devices.

In this thesis, the self-assembled vapor-liquid-solid growth of InP nanowires is studied. A catalyst-free method is employed using *in situ* deposited indium droplets as seeds for nanowire growth in metalorganic vapor phase epitaxy. The optical and

structural properties of the nanowires are studied using photoluminescence spectroscopy and electron microscopy. Also conventional vapor-liquid-solid growth of InP nanowires using catalytic gold nanoparticles is examined. The thesis is divided into five sections. After this introduction, the fabrication and applications of semiconductor nanowires are reviewed in section 2. Section 3 introduces the experimental methods used in this work for sample growth and characterization, and in section 4, the results of the work are introduced and discussed in context with the results of other groups. Finally, a summary and an outlook is given in section 6. The publications included in this dissertation are attached at the end after the references.

2 Semiconductor nanowires

In this section, the vapor-liquid-solid growth method used in this work is introduced along with a few other methods and nanowire devices.

2.1 Vapor-liquid-solid growth

Self-assembled fabrication methods of free-standing semiconducting nanowires can be divided into a few distinct groups. Some of them are categorized in Fig. 2.1. In 1964, Wagner and Ellis [1] proposed the vapor-liquid-solid (VLS) method for silicon whisker growth from $SiCl_4$ vapor on a silicon substrate. In this method, gold particles are placed on the substrate surface. At high enough temperatures the eutectic gold-silicon alloy is in liquid form as a droplet that acts as an efficient sink for Si atoms from the vapor [5]. As the liquid becomes supersaturated, silicon is incorporated in a crystal lattice at the liquid-solid interface below the liquid droplet, and as a result of the whole process, a whisker is formed, and the droplet floats at the tip. Deposition on solid surfaces is kinetically hindered. The process of nanowire fabrication using VLS is depicted in Fig. 2.2. The metallic droplet at the tip of an as-grown whisker is a characteristic feature of VLS growth. Originally the whiskers in Wagner and Ellis' studies had diameters in the micron range and were observable using conventional optical microscopy. However, the same mechanism using gold droplets has been used for the growth of nanowires, *i.e.*, wire-like structures with diameters less than 100 nm and aspect ratios greater than $\sim$10, of numerous materials, such as GaAs [6], InP [Ref. 7 and publication V], and InAs [6] using, *e.g.*, metalorganic vapor phase epitaxy (MOVPE), chemical beam epitaxy, and molecular beam epitaxy. Gold is preferred as droplet material due to its low eutectic-forming temperatures of about 340 °C and 450 °C with gallium and indium [8], respectively, but there are other candidates as well. For example, growth of GaN nanowires has been demonstrated using indium, nickel, and iron droplets [9]. Although the liquid droplet in VLS growth is often referred to as a catalytic particle, no actual catalysis in the chemical sense, *i.e.*, lowering of the activation energy of a chemical reaction with the catalyst left unchanged, necessarily takes place. Instead, the droplet acts as a "physical catalyst" promoting vertical growth through efficient collection of nanowire constituent atoms and supersaturation and precipitation thereof [5, 10, 11]. However, chemical catalysis has been shown to take place in GaP nanowire growth

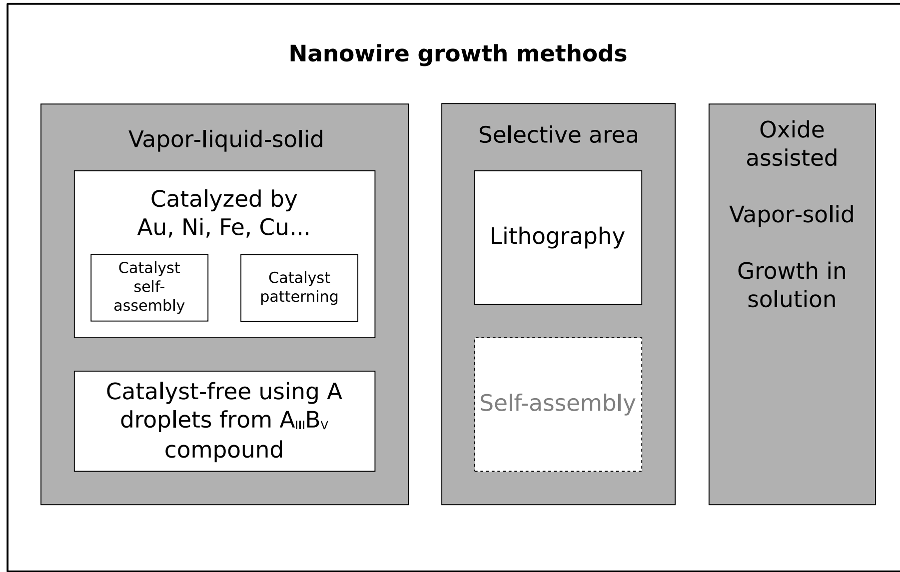

Figure 2.1: Some of the most commonly used methods for semiconductor nanowire fabrication.

using phosphine [12], and silicon and germanium nanowire growth using silane and germane, respectively [13].

The diameter of a typical VLS grown nanowire is a few tens of nanometers and the length up to several micrometers. Lateral strain relaxation in nanowires occurs elastically due to their small diameter [14]. Therefore, dislocations are not produced and heterojunctions between materials with highly different lattice constants, *e.g.*, GaAs, GaP, and InP nanowires on Si [15, 16] or InP nanowires on Ge [17] are enabled. Many groups have demonstrated also axially and radially heterostructured nanowires [18] in, *e.g.*, GaAs–InAs [19], InP–InAs [20, 21], GaAs–GaInP [22], GaAs–GaP [23], and GaP–GaAsP [24] materials. As shown on the left side of Fig. 2.1, the catalytic particles are either allowed to self-assemble, resulting in a random nanowire distribution, or they are patterned on the substrate to create ordered nanowire arrays. The former is achieved using, *e.g.*, metal evaporation and annealing [6], metal evaporation through block copolymer [25, 26] or porous alumina [27] templates, aerosols [28, 29], colloidal solutions [Ref. 7 and publication V], or metallocenes, although the techniques involving block copolymers and porous alumina can result in highly ordered structures. Patterning, on the other hand, can be done using nanosphere lithography [30, 31], electron beam lithography and lift-off [32], or nanoimprint lithography [33], for example. Laser assisted catalytic growth is based on laser ablation of a target that includes the nanowire material, such as Si, GaAs, or GaN, and the catalytic material [34–36], and results in nanowires, which are distributed on random sites upon condensation.

Under energy considerations, the onset of VLS growth is governed by the surface free energy of the liquid-solid interface itself and the energy of its edge [37, 38]. Depend-

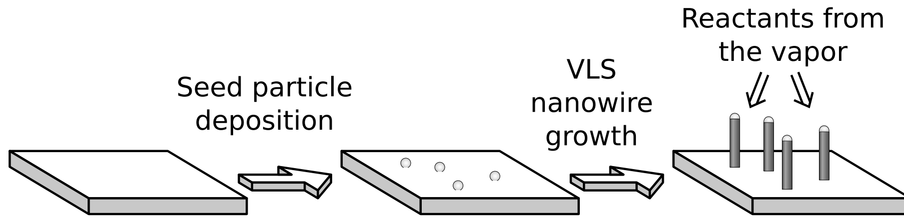

Figure 2.2: Nanowire fabrication using the VLS growth method.

ing on the liquid droplet diameter, one or the other dominates. For homoepitaxial silicon nanowires the critical diameter is about 20 nm. The interfacial energy dominates at large diameters, the edge energy at small ones. In zinc-blende III-V and II-VI compound semiconductors {111}B surfaces have the lowest free energy [39, 40]. Thus, with large liquid droplets the preferred growth direction is ⟨111⟩B and vertical nanowires can be grown on (111)B oriented substrates. In the case of III-V nanowire growth on silicon or germanium [15, 17], it remains unclear whether the growth direction is ⟨111⟩A or ⟨111⟩B since this polarity cannot be directly inferred from the orientation of the non-polar substrate. Most of epitaxial VLS nanowire studies today are carried out on (111) substrates. Growth in ⟨111⟩ direction has, however, a drawback: formation of twin stacking faults or rotational twins [41]. A zinc-blende crystal structure can be considered as a stacked sequence of three different diatomic layers in the ⟨111⟩ direction: $ABCABCABC\dots$. At a twin stacking fault this sequence is broken and changed into, *e.g.*, $AB\bar{A}\bar{B}\bar{C}\bar{A}\bar{B}\bar{C}\dots$ [42]. This is illustrated in Figs. 2.3(a) and 2.3(b) with a high-resolution transmission electron microscopy image of an InP nanowire and corresponding ball-and-stick models of the crystal structures. After the stacking fault the crystal structure is rotated 60° or 180° around the [111] axis [43]. Since creating these twin stacking faults does not result in dangling bonds in the final lattice, their formation energy is negligible and most nanowires with their growth axis in the ⟨111⟩ direction have a high number of twin stacking faults per unit length. Moreover, a high enough number of them can result in a totally different stacking sequence ($ABABABAB\dots$), which actually corresponds to the hexagonal wurtzite crystal structure in [0001] direction [6, 44, 45], as shown in Fig. 2.3(c). Although bulk III-V semiconductors typically crystallize in the zinc-blende form, stable wurtzite phases are encountered in nanowires [46, 47]. Of course, there can be stacking faults in hexagonal phases, too [48]. It has been shown that the twinning phenomenon can be controlled somewhat by the growth parameters [43, 44, 49].

2.2 Catalyst-free nanowire growth

Despite the fact that catalytic nanoparticles are commonly used for nanowire fabrication, there are some drawbacks associated with the use of catalysts. First, incorporation of the catalytic material in the nanowire directly or through diffusion [50]

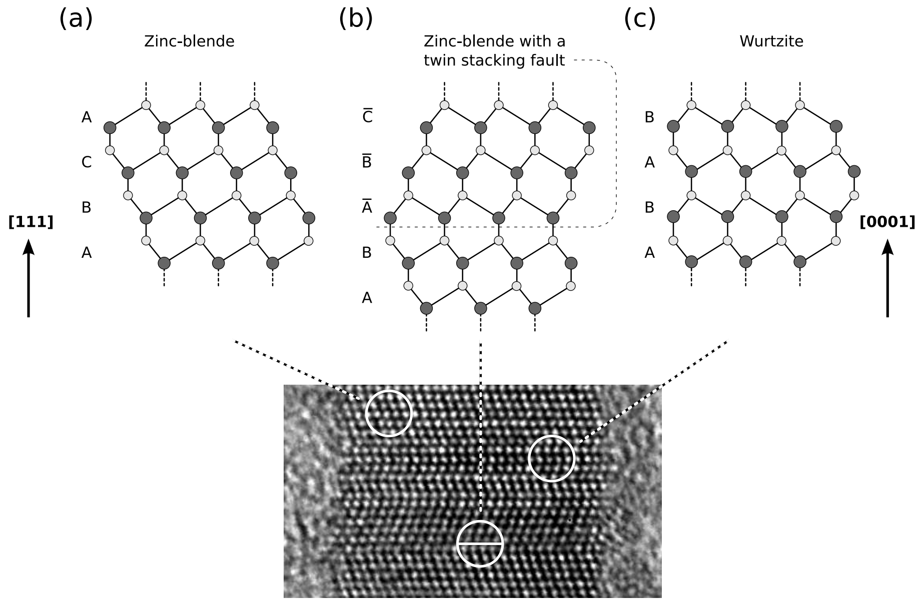

Figure 2.3: Simplified plane projection of (a) a perfect zinc-blende crystal structure, (b) a zinc-blende structure with a single 180° twin stacking fault, and (c) a wurtzite crystal structure. The structures are also indicated in a high-resolution transmission electron microscopy image of an InP nanowire.

can be detrimental in optoelectronic applications. Second, producing the nanoparticles on the substrate using the methods listed above may require some processing effort prior to the actual nanowire growth. In catalyst-free VLS growth techniques, the substrate surface is modified typically *in situ* to support nanowire growth without using third-party materials, such as gold. The exact way of the modification depends on the material system and fabrication equipment. For example, MOVPE growth of GaN and InN nanowires on sapphire has been demonstrated using a single-molecule precursor, which during initial decomposition produces metallic droplets that can seed subsequent nanowire growth [51, 52]. In reactive vapor transport experiments, catalyst-free growth of InN nanowires is achieved by initial deposition of InN nanocrystals or indium droplets [53]. In publications I, II, III, and IV, the *in situ* modification of InP surface by MOVPE using indium droplets to seed vertical nanowire growth [54] has been investigated. A similar growth method has been demonstrated also for ZnO [55] and (Al)GaN [56–58] nanowires using zinc and gallium droplets, respectively. The main point in these catalyst-free methods is to seed the growth of, *e.g.*, $A_{III}B_{V}$ or $A_{II}B_{VI}$ compound semiconductor nanowires by metallic nanoparticles of material A [59]. Using the catalyst-free method places some tighter restrictions on the growth parameters and material compositions outside binary compounds. Also new phenomena compared to, *e.g.*, gold-catalyzed VLS growth are observed, such as partial or complete incorporation or evaporation of the seed particle during growth [publications I and II] and possible homogeneous nucleation in the droplet. Nevertheless, using this technique allows the fabrication of 3D, 2D, and 1D structures, such as a strain-induced quantum dot structure [60]

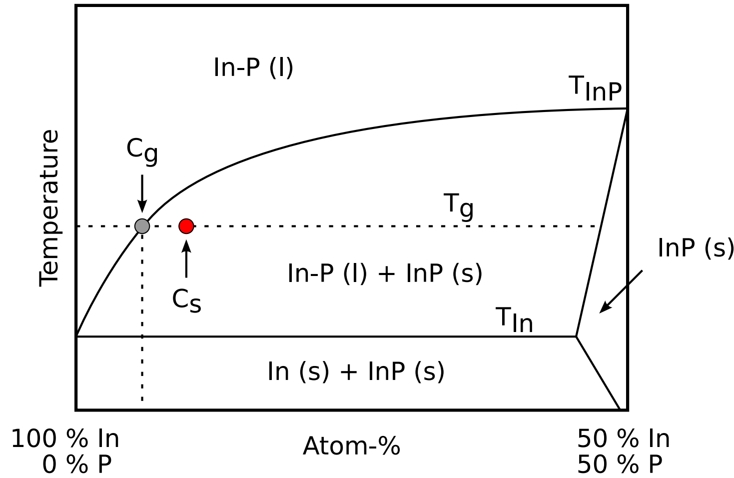

Figure 2.4: Composition–temperature phase diagram of the indium–phosphorus system (after Ref. 8). Solid and liquid phases have been marked with (s) and (l), respectively, and the melting points of indium and InP are denoted with T_{In} and T_{InP}, respectively. T_g is a temperature where the equilibrium and slightly supersaturated phosphorus concentration in In–P liquid are C_g and C_s, respectively. The composition axis is not linear.

with nanowires acting as stressors, within a single epitaxial growth run.

The VLS growth of nanowires through supersaturation and precipitation at the liquid–solid interface can be explained by considering the composition–temperature phase diagram of the binary system. The phase diagram for the indium–phosphorus system is shown in Fig. 2.4. As nanowire growth takes place in an indium rich melt, the composition considered ranges from pure indium to highly stoichiometric InP. The upper curve is a liquidus line, above which the system is in In–P liquid phase. The line itself is defined by temperatures at which the In–P liquid, vapor and the InP solid phases are in equilibrium. In the absence of a eutectic In–P alloy the liquidus line starts from the melting point of indium (157 °C), denoted with T_{In}, and increases monotonically up to the melting point of InP (1071 °C), denoted with T_{InP}. The triangular area near the stoichiometric InP composition is called the existence region, showing that slightly non-stoichiometric InP can exist in equilibrium. However, the deviation from exact stoichiometry is measured in parts per million and the width of the existence region is greatly exaggerated in the phase diagram. Similarly the width of the liquid phase region at small phosphorus compositions and temperatures below T_{InP} is wider than in reality.

Considering nanowire growth, let us assume that VLS growth takes place at temperature T_g and that there is neither indium supply from the gas phase nor indium evaporation from the droplet. Let us also assume that the liquid indium droplets are already present on the substrate surface. First, phosphorus is dissolved into the liquid indium droplets by (dissociative) adsorption from the gas phase and by

uptake from the substrate surface until the equilibrium phosphorus concentration C_g is reached in the In–P liquid. At 350 °C the equilibrium concentration is about 0.1 atom-% [8]. As more phosphorus is brought into the liquid droplet from the vapor phase, the phosphorus concentration is momentarily higher than the equilibrium value and a solid InP phase is precipitated at the liquid–solid interface. However, for each precipitated phosphorus atom one indium atom from the liquid is also incorporated into the lattice. Eventually the indium solvent is depleted and a short, highly tapered nanowire is grown, assuming that the growth of vertical nanowires is energetically favored. Next, let us consider adding an indium supply through the gas phase. A constant supersaturation, *i.e.*, a phosphorus concentration $C_s > C_g$, is maintained in the In–P liquid when the consumption of indium and phosphorus in the precipitation of solid InP is balanced by the supply directly from the gas phase and possibly by surface diffusion. If the indium supply is deficient, the phosphorus concentration of the whole system increases constantly and, again, the droplet is eventually consumed during nanowire growth. On the other hand, if the indium supply is higher than required for InP precipitation, phosphorus can be dissolved from the solid InP phase and indium is aggregated in the droplet. Another effect to be taken into account is that there is a concentration gradient in the liquid depending on the rate of phosphorus adsorption, precipitation and diffusion. The highest concentration is at the vapor–liquid interface, and at the liquid–solid interface the supersaturation is almost zero. The precipitation of solid InP is fed by phosphorus diffusion across the gradient.

Similar phase diagrams for systems such as gold–silicon can be used for VLS growth using third-party catalytic materials. However, the supersaturation and precipitation are somewhat different since there is no significant incorporation of gold into the growing lattice. Thus, the dynamics of returning to equilibrium concentration in the liquid are different, too.

2.3 Other growth mechanisms

Another epitaxial method for nanowire fabrication is selective-area (SA) growth (sometimes also referred to as catalyst-free growth in the literature), also shown in Fig. 2.1. In SA growth the substrate surface is templated using a mask with (circular) openings, and during subsequent growth nanowires emerge from the openings. This method has been demonstrated for, *e.g.*, GaAs, InAs, and InP [44, 47, 61, 62] nanowires using a SiO_2 template. The growth anisotropy necessary for nanowire formation arises from preferred diffusion and low sticking probability on {110} facets and incorporation on {111} planes. The size and position of the openings are typically defined using electron beam lithography, which is a rather time-consuming process and, thus, sets an upper limit for the practical size of the nanowire array and scalability; patterning whole wafers, for example, is not feasible. Nevertheless, it enables exact positioning of single nanowires in a small scale. Also, there

is no unwanted incorporation of third-party catalytic materials in the nanowires. It might also be possible to use porous alumina layers as self-assembled masks for selective-area growth, eliminating the slow lithography process.

The vapor-solid (VS) method is analogous to VLS but without the liquid droplet. For example, thermal evaporation of gallium at 300 °C within a supply of oxygen results in Ga_2O_3 nanowire growth on cooled surfaces [63]. Typically, VS growth is used to produce semiconducting metal oxide nanostructures [64]. Based on studies on low-temperature gold nanoparticle catalyzed growth of InAs nanowires, it has been proposed that the catalytic particle can be in solid state during growth, resulting in vapor-solid-solid (VSS) growth [65]. Oxide-assisted growth, like VS growth, also relies on thermal evaporation of source materials [66]. However, the evaporated materials are oxides, such as silicon monoxides for silicon nanowire growth. During growth, a semi-liquid SiO_x layer acts as a sink for silicon atoms in a similar way than the liquid droplet in VLS growth. Lateral growth is prevented by a solid SiO_2 shell. The shell is a drawback of the method along with a broad diameter distribution of resulting nanowires.

For nanowire growth in a large scale, solution growth methods can be used. Solution growth of ZnO nanowires has been demonstrated on various substrates using pre-deposited ZnO seed particles [67]. In addition to easily scalable production, another advantage of solution based growth methods compared to the methods above is the low growth temperature, typically below 100 °C. However, controlling the growth direction is challenging.

2.4 Nanowire devices and applications

Devices based on semiconducting nanowires using intricate contacting by electron beam lithography have been rather abundant in the literature after a p-n junction in a GaAs nanowire was demonstrated for the first time in 1992 [68]. Just to name a few devices, field-effect transistors (GaN [69], InP [70]), resonant tunneling diodes (InAs/InP [71]), light-emitting diodes (InP [70]), lasing structures (CdS [72]), optical modulators (GaN [73]) and single-electron memories (InAs/InP [74]) have been demonstrated. Sometimes nanowires can remain freely standing on the substrate and the substrate is used as one contact to create, *e.g.*, vertical wrap-gated InP nanowire transistors [75]. Even in this approach, the top contact of individual nanowires still remains a problem. In one solution metallic nanoparticles are attracted to as-grown nanowire tips using an electric field to eventually form a conducting film [76]. Another solution is to partially surround the nanowires with a dielectric layer, such as spin-on-glass, and use normal metallization by evaporation for contacting [68]. Both of these methods are, however, used only for contacting an ensemble of nanowires.

Optically pumped lasing has been demonstrated in single GaN [73, 77] and ZnO [78] nanowires, where the nanowire acts also as a waveguide. In addition, nanowires are highly suitable for sensing applications due to their large surface-to-volume ratio, giving them a high sensitivity and fast response to adsorbed molecules modifying their electrical [79] and optical [80] properties. For example, silicon nanowires have been used for highly sensitive DNA [81] and HCl and NH_3 detection [82], and ZnO nanowires for ethanol sensing [79]. There is a strong polarization anisotropy in the optical properties of nanowires due to the large dielectric contrast between the nanowire and the surrounding environment. Exploiting this phenomenon, polarization sensitive photodetectors have been demonstrated using InP nanowires [83].

Just being able to grow heterostructured semiconductor nanowires on a substrate does not automatically result in useful applications. The key to successful deployment is the ability to assemble individual nanowires into functional groups and meaningful architectures by correct positioning and electrical connectivity, similarly to the way diodes, resistors and light-emitting diodes are laid out and connected to each other on a printed circuit board. Aligning semiconductor nanowires into large arrays has been demonstrated using fluid flow approaches [84] and the Langmuir–Blodgett technique [85]. Aligned nanowire arrays can be used as sacrificial masks for further nanolithography [86]. Logic gates comprised of small arrays of aligned Si and GaN nanowires have been demonstrated [87], although with electrical contacts by electron lithography. If precise contacting of individual nanowires is not needed, the statistical nature of the Langmuir–Blodgett films can be exploited for simplified and easily scalable contacting [88]. It remains a challenge to find reliable and reproducible methods for nanowire fabrication, manipulation, and integration into functional devices.

3 Experimental methods

This section gives a brief overview of the nanowire fabrication and characterization methods used in this work.

3.1 Metalorganic vapor phase epitaxy

In epitaxial semiconductor growth techniques, the lattice structure of the underlying crystal, such as a substrate, is replicated in the growing layer – in an ideal case. In metalorganic vapor phase epitaxy (MOVPE), the constituent atoms of the layer are provided from metalorganic precursor vapors. Examples of such precursors are trimethylindium (TMI), trimethylgallium (TMG), tertiarybutylphosphine (TBP), and tertiarybutylarsine (TBA), all of which are typically used for the growth of III-V semiconductors, such as GaInAsP. A schematic representation of the MOVPE system used for sample fabrication in this work is shown in Fig. 3.1.

The system consists of gas lines and a horizontal quartz glass reactor. Hydrogen is passed through bubblers containing the metalorganic precursors, and the precursor vapors are brought into the reactor within a hydrogen or nitrogen carrier gas. The gas flows are computer controlled using mass flow controllers, and the bubblers are located in temperature-stabilized baths to achieve a known vapor pressure for each metalorganic precursor. The substrate is located in the reactor on a graphite susceptor which is heated from below by a halogen lamp. Feedback for the heater is provided by a thermocouple located in the susceptor. The substrate surface temperature is a few tens of degrees lower than the thermocouple temperature. A typical growth temperature for the growth of two-dimensional, conventional III-V semiconductor layers is about 650 °C. Higher temperatures are required for the nitrides.

The main processes in MOVPE growth are mass transport from the vapor phase to the substrate surface, precursor molecule decomposition and atom adsorption, atom diffusion on the substrate surface, and atom desorption from the substrate surface. One or more of these processes are the limiting factors during crystal growth, and, thus, different growth temperature regimes can be defined. Vapor-liquid-solid growth of InP nanowires by MOVPE with [publication V] or without

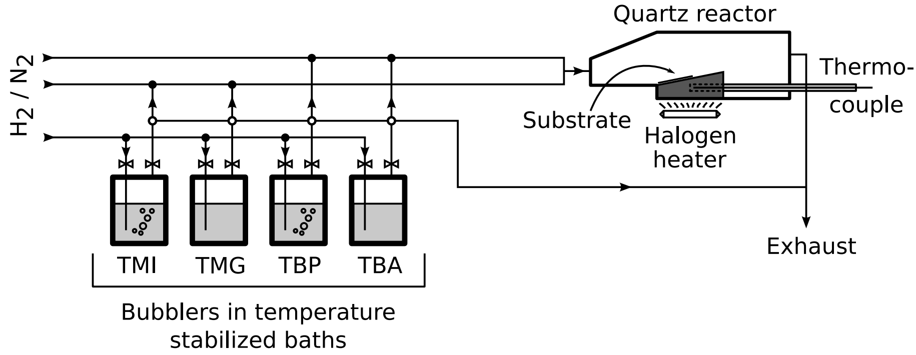

Figure 3.1: Schematic representation of the metalorganic vapor phase epitaxy system used in this work.

[publications I–IV] metal catalyst particles typically takes place at temperatures well below 500 °C. At these temperatures growth is limited by reaction kinetics. This is important in nanowire fabrication, since atoms can contribute to the growth of a single nanowire only if they are able to reach the liquid droplet at the nanowire tip by surface diffusion or by direct impingement [11]. Moreover, the metalorganic molecules decompose incompletely at low temperatures. For example, the decomposition temperatures of TMI and TBP molecules are 325 °C and 475 °C, respectively. At a typical growth temperature for catalyst-free InP nanowires, 350 °C, the decomposition efficiency of TMI is highly dependent on temperature and most of the TBP molecules do not decompose at all [89]. However, if real chemical catalytic action of metal nanoparticle catalysts is to be expected, the decomposition temperature of the metalorganic molecules can be considerably lower [12].

3.2 Optical characterization

One of the key elements in determining the feasibility of using semiconductor nanowires in optoelectronic applications is the assessment of their optical activity. From an application point of view, electroluminescence measurements from single or even an ensemble of nanowires provides the most accurate information about the luminescence wavelength, intensity, and dynamics. However, this approach requires the fabrication of a p-n junction in the nanowires, and, in the case of single-nanowire measurements, some rather complicated electrical contacting. In this work, the optical activity of nanowires was studied by photoluminescence (PL) spectroscopy in continuous-wave and time-resolved arrangements. A schematic representation of the PL setup used for continuous-wave measurements at room temperature for publications I, II, and V is shown in Fig. 3.2. The 532 nm line from a frequency-doubled Nd:YVO_4 laser was used for excitation. The excitation light was focused on the sample using a microscope objective. The same objective was used to collect the luminescence from the nanowires to be dispersed in a monochromator. In the

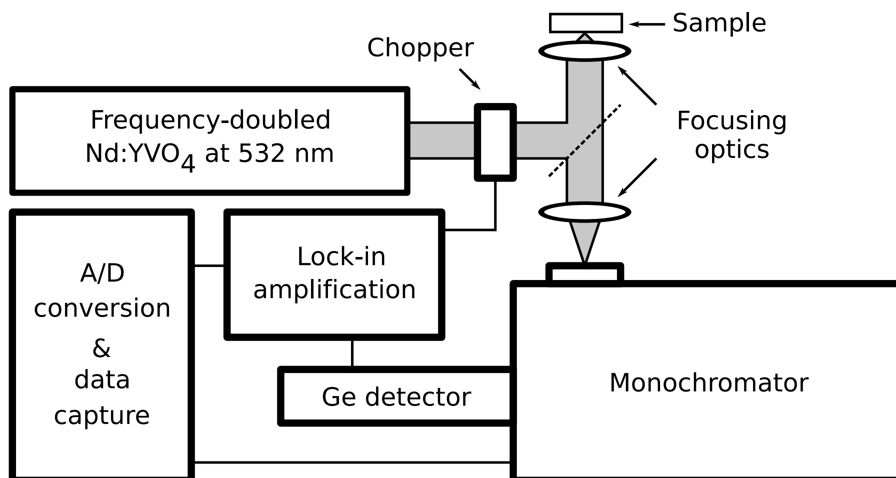

Figure 3.2: Schematic representation of the photoluminescence setup used for the optical characterization of semiconductor nanowires.

PL measurements for publication V separate focusing and collection optics were used. Typical excitation intensity at the sample was about 100 Wcm^{-2}. A liquid nitrogen cooled germanium detector and standard lock-in techniques were used for signal detection and data capture.

Time-resolved photoluminescence (TRPL) and some of the continuous-wave PL measurements in this work [publications III and IV] were performed using the setup illustrated in Fig. 3.3. A mode-locked titanium-sapphire laser operating at 800 nm was pumped using a frequency-doubled Nd:YVO_4 laser at 532 nm. To achieve better excitation light absorption in the InP nanowires, the pulses at the output of the mode-locked laser were frequency-doubled to 400 nm using an optically nonlinear bismuth triborate (BIBO) crystal. The pulse repetition rate of the titanium-sapphire laser was 76 MHz, estimated pulse width a few hundred femtoseconds, and the average excitation intensity of the second harmonic at the sample 10 Wcm^{-2}. The PL signal was collimated, focused, dispersed in a monochromator and detected using a Peltier-cooled microchannel plate photomultiplier tube along with single-photon counting electronics. In continuous-wave PL measurements using this setup, the setup was amended with an optical chopper and the detector signal was taken to a lock-in amplifier like in the continuous-wave setup in Fig. 3.2. The sample was inside a closed-cycle helium cryostat with a temperature range of 9–350 K.

Since the PL intensity of as-grown nanowires can be low due to possible surface recombination effects, or the fact that their areal density is low, discerning the nanowire PL signal from the substrate PL signal can be difficult. This is the case especially with homoepitaxial nanowires. In this work the problem was solved simply by detaching nanowires from the substrate using adhesive tape. The effectiveness of the method can be seen in Fig. 3.4 showing the PL spectra measured from the reference (111)B InP substrate, the gold-nanoparticle-catalyzed InP nanowires on

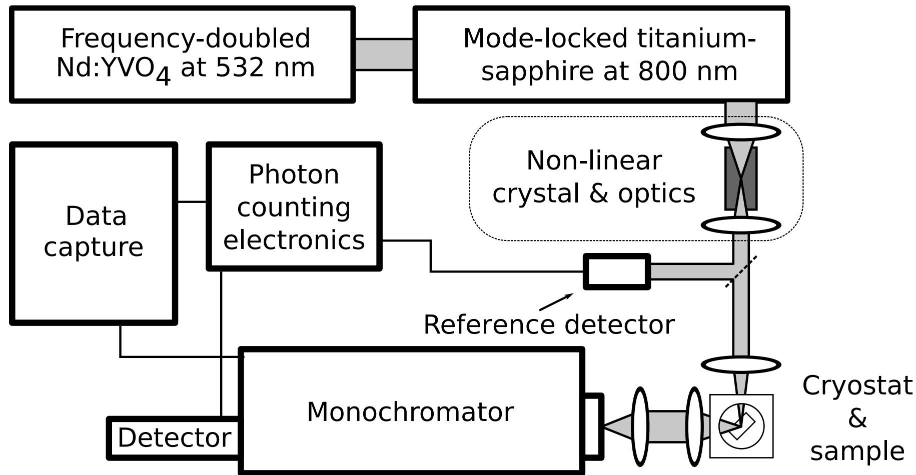

Figure 3.3: Schematic representation of the experimental setup for time-resolved photoluminescence measurements.

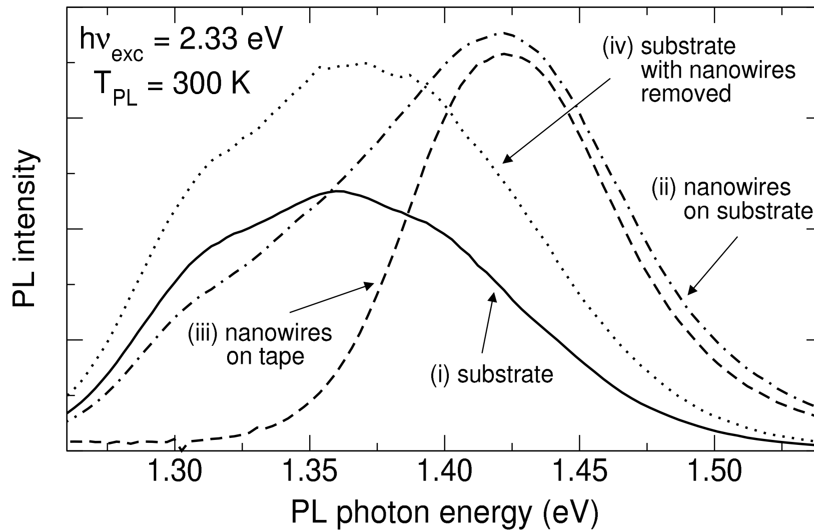

Figure 3.4: Room temperature PL spectra from (i) (111)B InP substrate, (ii) as-grown InP nanowires on substrate, (iii) nanowires on adhesive tape, and (iv) InP substrate with nanowires removed. Intensities are not to scale [publication V].

and off the substrate, and the substrate with the nanowires removed. Although the signal from the nanowires is visible even when measured on the substrate, removing the nanowires from the substrate makes the spectrum clearer and enables, *e.g.*, peak width analysis without peak fitting. Moreover, it would be virtually impossible to measure TRPL from nanowires on the substrate since at a given wavelength there would be contribution from both the nanowires and the substrate.

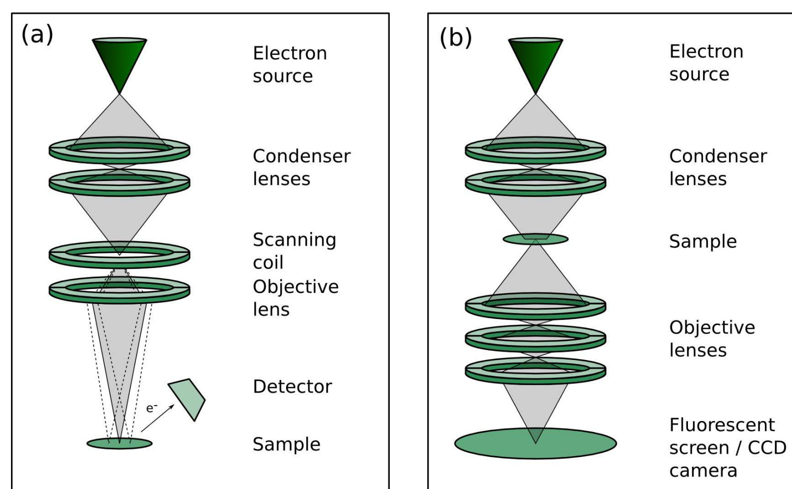

Figure 3.5: Simplified electron optics of a (a) scanning electron microscope and (b) transmission electron microscope.

3.3 Electron microscopy

In this work, scanning electron microscopy (SEM) and high-resolution transmission electron microscopy (TEM) were used for structural sample characterization. SEM gives a good general overview of nanowire homogeneity over a substrate and was used to measure nanowire length and diameter histograms, areal densities, and growth orientations and angles with respect to the substrate surface. A simplified illustration of the imaging process in SEM is shown in Fig. 3.5(a). A beam of electrons is emitted from an electron source, such as a heated filament. Typical electron acceleration voltage range is 1–20 kV. The beam is shaped using electromagnetic condenser lenses and focused on the sample by the objective lens. The focused spot is scanned on the sample using a coil, and secondary electrons emitted by atoms near the measurement spot are detected. The final image is formed by combining position information from the scanning coil driver with the detector signal. Also back-scattered electrons can be used for imaging. The resolution of SEM is typically a few nanometers.

Details about the morphology of single nanowires, their crystal structure and crystalline quality are obtainable by TEM imaging and electron diffraction. Compared to SEM, also more accurate measurements of nanowire dimensions are possible due to the higher resolution. With atomic resolution being available in high-resolution TEM images, information on the lattice periodicity can be gained also by calculating the two-dimensional fast Fourier transform (FFT) of the image. Moreover, with energy dispersive x-ray spectroscopy (EDS) it is possible to measure the chemical composition of nanowires. Due to their nanoscale size, usually nanowires can be directly observed with a transmission electron microscope without sample preparation. In this work, nanowires were transferred on commercially available copper

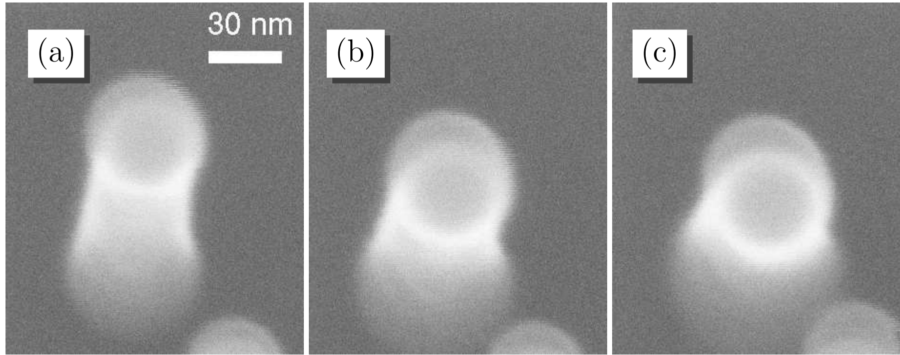

Figure 3.6: Electron-beam induced damage on InP nanowires during SEM observation at (a) $t \simeq 0$ s, (b) $t \simeq 20$ s, and (c) $t \simeq 40$ s.

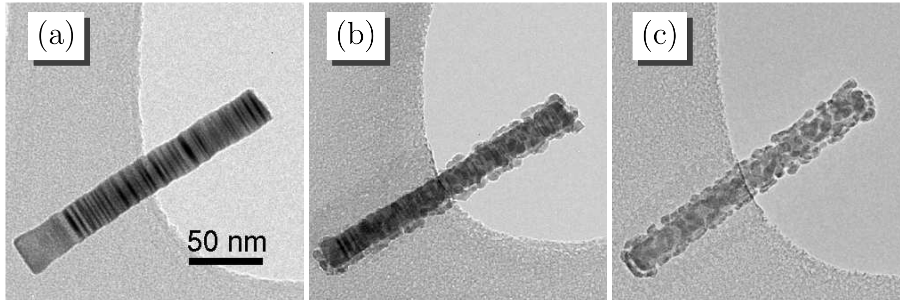

Figure 3.7: Electron-beam induced damage on InP nanowires during TEM imaging at (a) $t \simeq 0$ s, (b) $t \simeq 120$ s, and (c) $t \simeq 240$ s.

TEM grids covered with holey carbon film by placing a grid on a substrate containing nanowires and moving it around on the surface. A schematic illustration of the imaging process in TEM is shown in Fig. 3.5(b). The sample is illuminated using a beam of highly energetic electrons through a group of electromagnetic condenser lenses. Typical electron acceleration voltage range is 200–400 kV for materials science, with point resolution up to 0.16–0.24 nm. An image of the sample is formed on a fluorescent screen and can be recorded with CCD cameras. Several lenses are combined to obtain high magnifications, up to 1 million in high-resolution TEM equipment, enabling imaging at atomic resolution.

Depending on the material, the electron beam can damage the sample when imaging a small area, *i.e.*, using high magnifications in SEM. This is clearly seen in the series of close-up images of a single catalyst-free-grown InP nanowire on InP in Fig 3.6, where the nanowire shape is changed significantly within 40 s of continuous imaging at 300000× magnification using a beam current of about 20 nA. However, at smaller magnifications that were used in this work for nanowire sample characterization, no obvious damage was observed. Electron beam induced damage was observed also during TEM imaging as shown in Fig. 3.7. The surface of a single catalyst-free-grown

InP nanowire changes significantly within a few minutes of continuous illumination at high magnifications, *e.g.*, above 300000×. The nanowire surface is transformed into nanocrystalline InP, preventing closer inspection of the crystal structure and diffraction from the nanowire core. The beam damage can be minimized by lowering the illumination intensity and avoiding unnecessary illumination. The missing indium droplet on the tip is due to a surface treatment of the nanowire in hydrofluoric acid rather than a consequence of the beam damage, as seen in Fig. 3.7(a). The susceptibility of a single nanowire for beam damage can depend on local strain or defect structure [90].

3.4 X-ray diffraction

X-ray diffraction (XRD) is a widely used characterization technique for crystalline materials. For epitaxially grown layered structures, XRD curves are used to determine the composition and thickness of each layer. Typically, $\omega/2\theta$ curves are measured around a known diffraction maximum of the substrate, and determination of layer parameters is done by fitting a theoretical curve to the measured one. Using XRD to characterize nanowires is a little more complicated due to reduced interaction volume and possibly random orientation with respect to the substrate. If the nanowire areal density is high and the orientation of each nanowire is random, the crystalline structure of the nanowires can be determined using methods similar to powder diffraction. If the number of nanowires per unit area is small, the signal-to-noise ratio may be too small. However, if all the nanowires are oriented the same way, like in publication V, it may be possible to get diffraction from the nanowires. The interpretation of the results can be complicated by contribution from the substrate. More information can be gained by measuring $\Delta\omega - \Delta(\omega/2\theta)$ diffraction maps.

4 Catalyst-free indium phosphide nanowires

4.1 Size-controlled growth on indium phosphide

A general MOVPE growth sequence of homoepitaxial catalyst-free InP nanowires used in this work is illustrated in Fig. 4.1. The main phases are oxide removal (650 °C), droplet deposition and nanowire growth (310–350 °C). The reactor was at atmospheric pressure and hydrogen was used as the carrier gas. Molar TMI flow was typically fixed at 5 μmol min^{-1}, and the molar V/III ratio was controlled by adjusting the group V precursor flow. Droplet deposition time was 15 s, and nanowire growth time was varied between 105 and 420 s.

A driving force for catalyst-free nanowire growth using *in situ* deposited droplets as seeds is the fact that it enables growth-time tailoring of nanowire properties. The effect of growth parameters on the dimensions of catalyst-free-grown InP nanowires was studied in publication I. First, the growth temperature dependence of the diameter of droplets and resulting nanowires was studied. SEM images of droplets and nanowires grown at 310–350 °C are shown in Fig. 4.2. No droplets were formed on the substrate without TMI during the droplet deposition step. Thus, the main source for indium is the precursor and not the substrate. The observed nanowires were categorized into three types. Type A nanowire is vertical with an indium droplet at the tip, and type B nanowire is vertical but highly tapered and missing the droplet. Nanowires of type C are inhomogeneous with differing diameters, lengths, and orientations with initial vertical growth. Nanowires representing each type are indicated by arrows in one of the SEM images in Fig. 4.2. When collecting statistics on nanowire length, only nanowires of type A were taken into account because their growth had not been terminated by the premature disappearance of the indium droplet during the deposition. The average length of type A nanowires grown at 350 °C for 210 s was about 550 nm resulting in a growth rate of about 2.6 nm/s. The areal density and diameter of the droplets and type A and B nanowires vs. growth temperature are plotted in Fig. 4.3. The nanowire diameter was measured at the base to enable nanowire and droplet diameter comparison and to get rid of the error due to tapering. Growth at 310 °C and 350 °C for 210 s resulted in average nanowire base diameters or about 23 nm and 45 nm, respectively. Droplet diameters are slightly larger than nanowire diameters as expected, except at the lowest temperature.

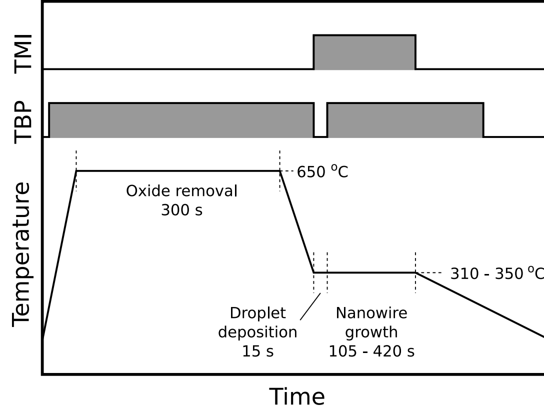

Figure 4.1: Temperature and group III (TMI) and group V (TBP) precursor sequencing during a catalyst-free growth run of InP nanowires.

Since the droplet material is one constituent in the binary compound, it is incorporated in the lattice as the nanowire grows, as explained in section 2. SEM images from nanowire samples grown at 350 °C for 210 s using nominal V/III molar ratios between 100 and 250 are shown in Fig. 4.4. The aggregation of indium in the droplets is evident from their increasing diameter with decreasing V/III ratio. Also the base diameter is slightly larger for nanowires grown at lower V/III ratios. That is probably due to additional indium aggregation in the droplet until phosphorus supersaturation is reached and vertical growth commences, since identical droplet deposition steps were used in all cases. Depending on the net flow of indium into the droplet its diameter either increases or decreases during growth resulting in nanowire tapering [54] and possibly eventual extinction of the droplet. No clear evidence of reverse tapering, *i.e.*, increasing of the droplet diameter due to indium aggregation during growth at small V/III ratios can be observed, possibly due to the short nanowire length. The average nanowire length increases from about 320 nm to 880 nm when the V/III ratio is increased from 100 to 250. Corresponding growth rates are about 1.5 and 4.2 nm/s. The increased growth rate can be due to increased phosphorus supersaturation in the droplet and faster phosphorus diffusion into the liquid–solid interface. Under the assumption that phosphorus reaches the liquid droplet only through direct impingement, the nanowire radius has no effect on the growth rate, unlike in group III surface diffusion limited MOVPE growth, where thin wires grow faster [29]. However, no definite conclusions about the dependence of the growth rate on nanowire diameter can be drawn here, since the composition of the vapor phase was different for each sample, and the nanowire diameter distribution was quite homogeneous. Moreover, the Gibbs–Thomson law [29] sets the lower limit for the diameter of the liquid indium droplet. With decreasing diameters the effective vapor pressure of the droplet material increases, and below the critical diameter it is higher than the partial pressure of indium in the vapor phase from the precursor and the droplet evaporates.

The tapering phenomenon in catalyst-free growth is fundamentally different from

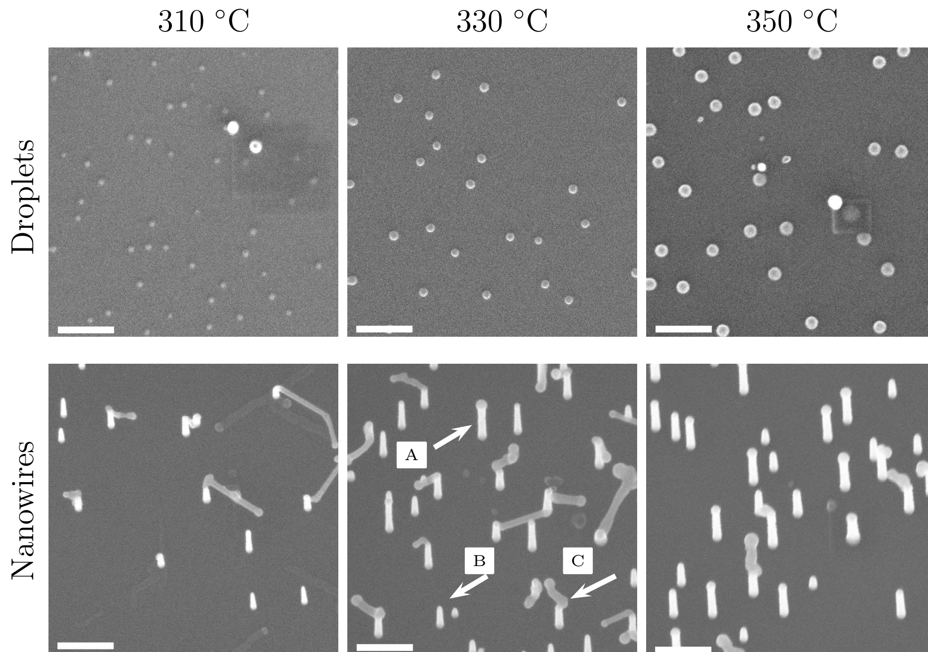

Figure 4.2: SEM images of indium droplets and droplet seeded InP nanowires grown on InP at different temperatures. Nanowires of type A, B, and C are indicated by arrows. Sample tilt is 10° and the scale bars correspond to 200 nm [publication I].

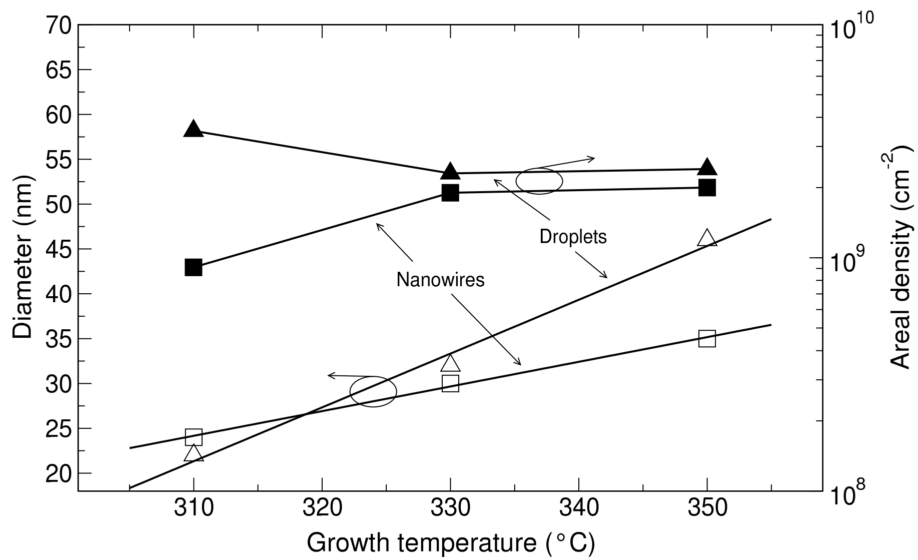

Figure 4.3: Areal density and diameter of indium droplets and InP nanowires seeded by indium droplets vs. growth temperature [publication I].

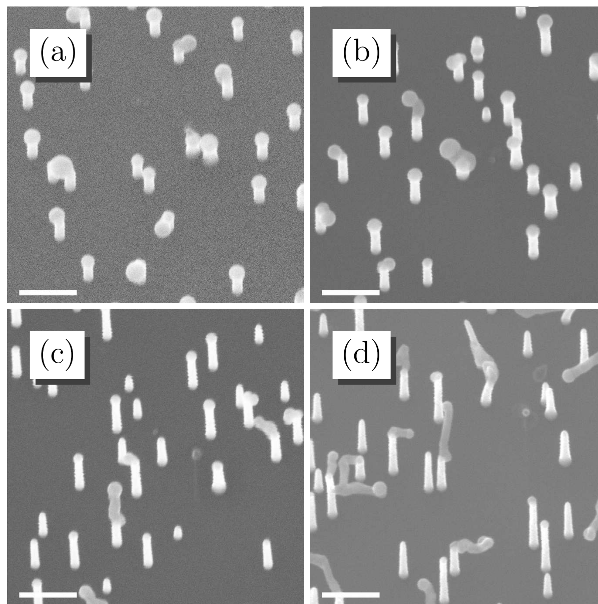

Figure 4.4: SEM images of catalyst-free-grown InP nanowire samples grown at 350 °C for 210 s with a nominal V/III molar ratio of (a) 100, (b) 150, (c) 200, and (d) 250. Sample tilt is 10°, and the scale bars represent 200 nm [publication I].

that in, *e.g.*, gold-nanoparticle-catalyzed growth, where tapering is believed to be caused mostly by competing lateral growth [6, 91], exploited for shell growth in core–shell structures. As this lateral growth takes place at about 100 °C higher temperatures [publication V], it is not an issue with catalyst-free growth. However, the level of supersaturation in the droplet also has an effect on its radius and, thus, can result in tapered growth [92, 93], too.

For homogeneous nanowire distributions, the areal density of type C nanowires should be minimized. The number of type C nanowires was significantly reduced when shorter growth times were used. A comparison of the areal densities of nanowires of different type as a function of growth time is shown in Fig. 4.5. The growth temperature and V/III ratio were 350 °C and 200, respectively. Samples with growth time of 105 s have practically no type C nanowires. As the growth time is increased, the number of type C nanowires increases. The total nanowire areal density remains roughly constant at $2 \cdot 10^9$ cm^{-2}, which is also the areal density of seeding indium droplets at the beginning of growth. Also the length of remaining type A nanowires increases in a roughly linear fashion with time. Therefore, an increasing number of vertical wires kink into type C as growth continues. In gold-nanoparticle-catalyzed VLS growth, where the growth rate is limited by the supply of group III atoms into the catalytic particle [29, 94], kinking has been proposed to happen when the nanowire length equals the migration length of group III atoms on the nanowire surface [93, 95]. At that point the flux into the catalyst changes, and the system is directed towards a new equilibrium. Here, however, the supply

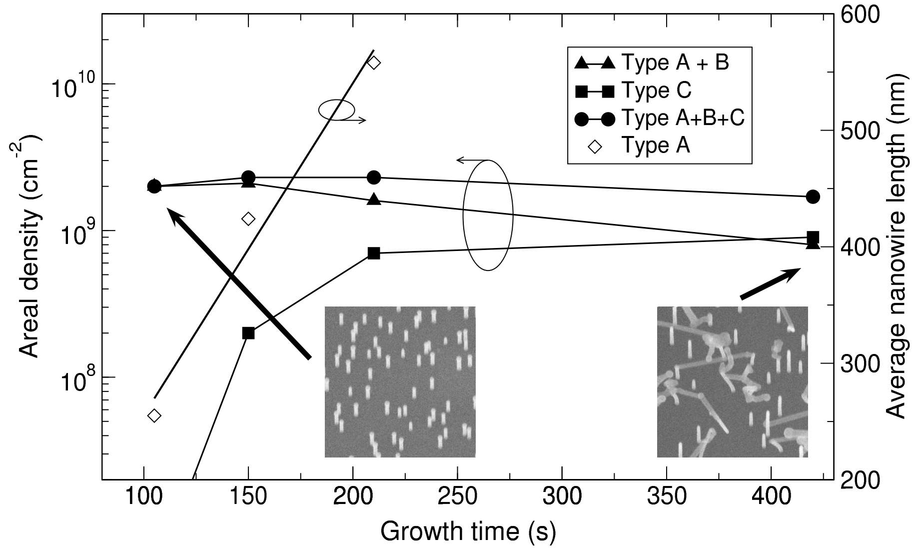

Figure 4.5: Areal density of vertical InP nanowires (types A and B), type C nanowires, their sum, and average type A nanowire length vs. growth time at 350 °C. SEM images from samples grown for 105 s and 420 s are shown as insets. The lines are guides for the eye.

of group III atoms should not be a problem. Group V atoms on the other hand, are considered highly volatile, and the supersaturation in the liquid droplet is fed only through direct impingement. Thus, the supersaturation should have no dependence on nanowire length. Nevertheless, kinking is observed. Moreover, according to Fig. 4.4, the kinking probability seems to be more closely related to growth time rather than actual nanowire length. One could argue that the kinking is, however, caused by changes in indium diffusion into the droplet and, thus, changes in its size and the level of supersaturation. The analysis is further complicated by the decomposition kinetics of metalorganic precursor molecules. In Ref. 54, InP nanowires up to several micrometers in length were grown at similar temperatures with the catalyst-free method, apparently without any kinking. However, the nanowire diameter was larger which can affect the mass transfer into the droplet, and the sources for indium and phosphorus were TMI and phosphine, respectively. In addition, the reactor pressure was lower. Using phosphine and lower pressures decreases the partial pressure of phosphorus in the vapor phase, which should decrease also the growth rate.

4.2 Nanowire growth on silicon

Semiconductor nanowires can be used to combine optically active III-V compounds with well established silicon technology since large lattice constant differences do

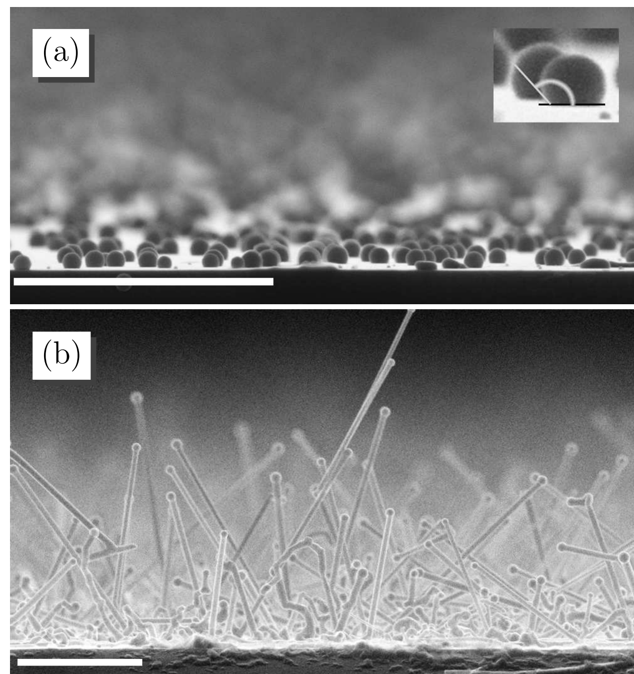

Figure 4.6: SEM image of (a) indium droplets and (b) InP nanowires on (111) Si. The scale bars correspond to 1 μm [publication II].

not prohibit epitaxial dislocation-free nanowire growth [15, 16]. Using the catalyst-free VLS process to fabricate InP nanowires on silicon was studied in publication II. The growth sequence was similar to the one used with InP substrates but the oxide removal step was omitted. No nanowire growth was observed on substrates etched in hydrofluoric acid and annealed under hydrogen before growth, a result similar to a previous report on silicon nanowire growth without catalytic particles [96]. This indicates that the native oxide plays a significant role in the initial growth process. Droplet deposition and nanowire growth was performed at 350 °C. SEM images of indium droplets and droplet-seeded InP nanowires on (111) Si substrate are shown in Fig. 4.6. The initial nanowire growth near the substrate surface has no clear direction and, thus, growth is not epitaxial. After a while a part of the nanowires reach a state of linear growth after which no kinking can be observed. The non-epitaxial growth on Si substrate with native oxide is in agreement with reports on III-V nanowire growth on silicon using gold nanoparticle catalysts [15, 97]. The average nanowire diameter was about 55 nm, and the average diameter of the droplet at the tip was about 90 nm. Assuming that the Gibbs–Thomson effect can be neglected [10, 29], although the partial pressures of indium and phosphorus in the vapor phase can be quite low, larger nanowire diameter should result in lower growth rate. Yet, the growth rate was almost ten times higher ($\sim$10–20 nm/s) on silicon than on InP substrates, resulting in average lengths of 1–2 μm.

As it was shown in publications I and II, catalyst-free VLS growth of size-controlled InP nanowires on InP and Si substrates is possible using *in situ* deposited indium

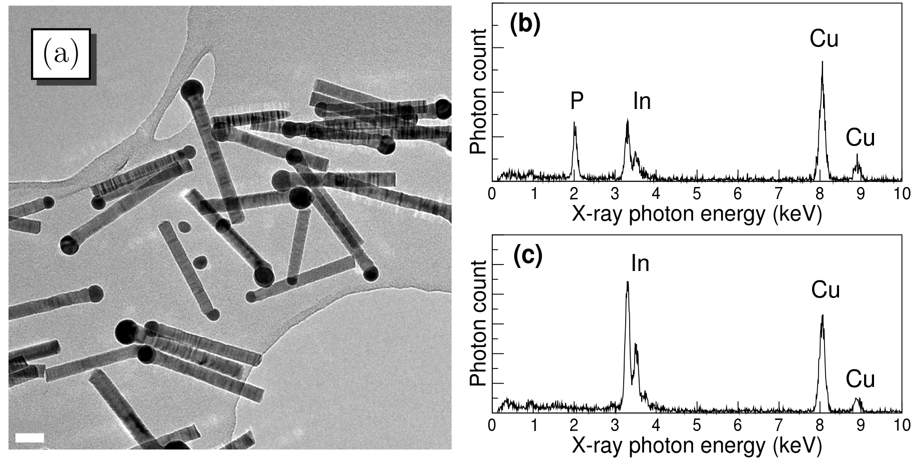

Figure 4.7: (a) Low-magnification TEM image exhibiting originally type A and B InP nanowires. The scale bar corresponds to 50 nm. EDS spectra measured from (b) InP nanowire core and (c) droplet.

droplets as seeds for the nanowire growth, enabling growth-time tailoring of nanowire properties. For example, patterning the substrate with nanowires of different diameters is possible by creating local temperature variations or gradients on the substrate surface. Nanowires with tapered and reverse tapered segments could be grown by changing the V/III ratio during growth. However, since the length of vertical type A nanowires on InP is limited due to the appearance of type C nanowires, the number and size of tapered segments would be limited, too. Nevertheless, tapering could be exploited to create, *e.g.*, quantum dot chains within suitably narrow nanowires. This kind of flexibility does not exist in conventional VLS growth.

4.3 Crystal structure of catalyst-free-grown nanowires

Figure 4.7(a) shows a low-magnification TEM image of type A and B InP nanowires grown on (111)B InP substrate. Depending on their orientation with respect to the electron beam, twin stacking faults are visible in some nanowires as lines perpendicular to nanowire axis. EDS spectra measured from the nanowire core and the droplet are shown in Figs. 4.7(b) and 4.7(c), respectively. The copper signals in both spectra are from the TEM grid. In the spectrum measured at the core, peaks arising from phosphorus and indium can be observed. By correlating the photon count related to both species with actual atomic concentrations, the core material can be quantified expectedly as stoichiometric InP. The droplet spectrum is missing the phosphorus related peaks indicating a phosphorus concentration of less than one atomic percent, given the accuracy of the EDS measurement.

The crystalline growth direction of InP nanowires with respect to the substrate was

studied in detail in publication III. The nanowire growth direction in relation to the atomic planes of the zinc-blende lattice is illustrated using a polyhedron bounded by the low-index planes of the lattice (Miller cube). By comparing the growth direction of nanowires on a known substrate with the directions of the normals to the planes of the Miller cube and assuming epitaxial growth, the crystalline orientation of the nanowires can be deduced from SEM images. This is shown Figs. 4.8(a)–(d), where a plan-view and a tilted view SEM image of nanowires grown on (111)B InP substrate is compared to the Miller cube amended with nanowires with their axes in ⟨111⟩B directions. As only tips are visible at 0° tilt and increasing the tilt reveals the trunks, the nanowires have grown in [111]B direction. However, zinc-blende and wurtzite structures cannot be distinguished from each other in SEM images. The high-resolution TEM image and the two-dimensional FFT in Fig. 4.8(e) confirm that the crystal structure is cubic zinc-blende with twin stacking faults. The FFT spots can be indexed to a cubic structure and twin spots can be observed for, *e.g.*, (002) spots. Zinc-blende blocks with one orientation are highlighted in the dark-field TEM image along with an electron diffraction pattern in Fig. 4.8(f).

As nanowires grown in ⟨111⟩ directions are plagued with twin stacking faults, making nanowires grow in other crystalline directions would be beneficial. One way of achieving that could be by using different substrate orientations. Growth of homoepitaxial nanowires free of twin stacking faults with ⟨110⟩ axes on (001) GaAs [98] and with ⟨001⟩ axes on (001) InP [99] has been demonstrated, possibly using a chemical treatment of the substrate surface to promote vertical growth. In publication III, catalyst-free InP nanowire growth was studied on (111)A, (110), and (001) InP substrates with the exact same growth parameters that were used for vertical nanowire growth on (111)B InP substrate. The SEM images with corresponding Miller cubes are shown in Fig. 4.9. By comparing the number of different azimuthal growth directions and the elevation angle of the nanowires, and again assuming epitaxial growth, it was concluded that the nanowire growth direction was ⟨111⟩B regardless of the substrate orientation on (111)A and (110) substrates. Nanowire growth was not observed on (001) substrate. Instead, plateau-like features were formed along the substrate surface in two available azimuthal directions, *i.e.*, in the direction of the projections of available ⟨111⟩B directions on the substrate surface. Interestingly, some indirect evidence of initial nanowire growth in the [111]A direction on (111)A substrate was found by closer inspection of the number of different azimuthal nanowire growth directions. There are three ⟨111⟩B directions pointing out of the substrate plane on (111)A substrate. However, growth in six distinct directions in three antiparallel pairs was observed. This was proposed to be explained by initial nanowire growth perpendicularly to the substrate surface in [111]A direction and the formation of a 60° or 180° twin stacking fault before kinking into one of the energetically favorable ⟨111⟩B directions. This is illustrated in Fig. 4.10. After kinking the nanowires grow in antiparallel azimuthal directions making the phenomenon difficult to observe in plan-view SEM images.

Since the nanowire crystalline structure cannot without a doubt be identified by

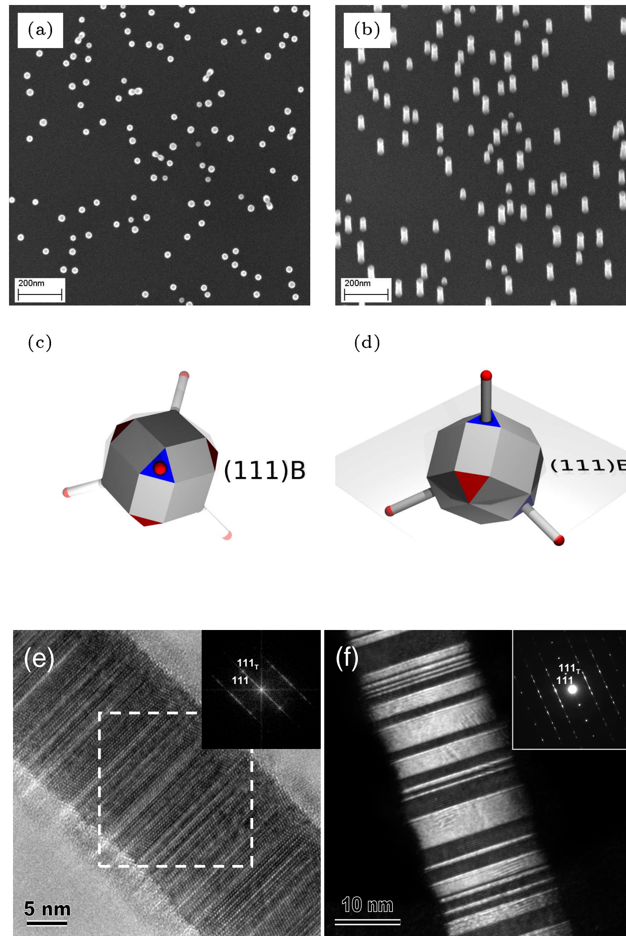

Figure 4.8: SEM image of InP nanowires grown on (111)B substrate at (a) 0° tilt and (b) 15° tilt. Corresponding Miller cubes illustrating the growth direction with respect to the low-index lattice planes are shown in (c) and (d). A high-resolution TEM image of an InP nanowire grown on InP (111)B substrate is shown in (e), and a dark-field TEM image of the same nanowire in (f). The insets show the FFT calculated from the framed region and an electron diffraction pattern, respectively [publication III].

SEM image analysis, TEM images were captured from nanowires grown on (111)A and (110) substrates. The images along with two-dimensional FFTs are shown in Fig. 4.11. The nanowire crystalline structure on both substrates was zinc-blende with the growth axis parallel to the ⟨111⟩B direction. There was also clear evidence of edge faceting with the periodicity of the twin stacking faults. Even if the nanowires grown on different substrate orientations are structurally similar, the growth process itself is not. This is evident from the SEM images in Figs. 4.8 and 4.9, where clear differences in nanowire diameters, lengths and areal densities can be observed. Diameter histograms for nanowires grown on (111)B, (111)A, and (110) substrates are shown in Fig. 4.12. Nanowires on (111)B substrate have the narrowest diameter distribution. Distributions of nanowires grown on (111)A and (110) sub-

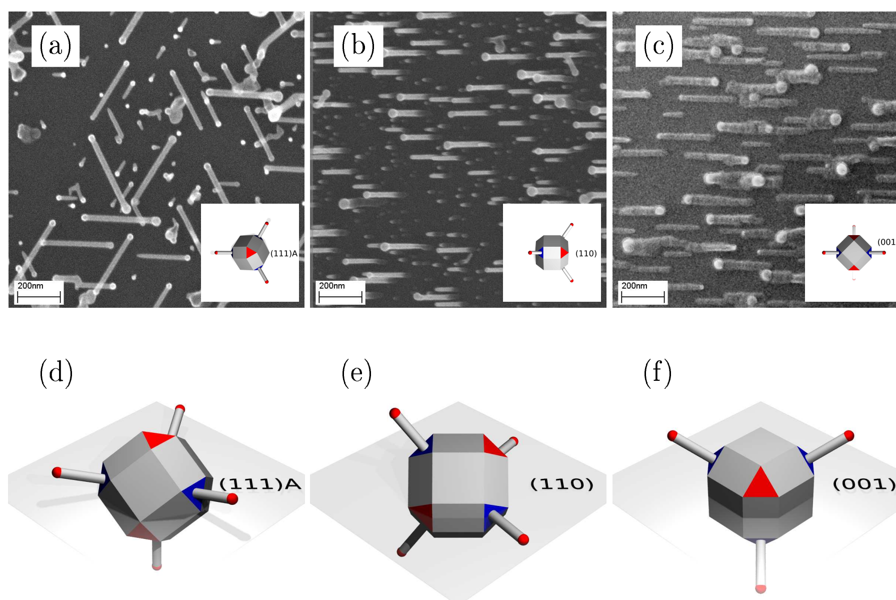

Figure 4.9: SEM image at 0° tilt of InP nanowires grown on (a) (111)A, (b) (110), and (c) (001). Corresponding Miller cubes are shown in the insets. Tilted Miller cubes illustrating available ⟨111⟩B growth directions on (111)A, (110), and (001) substrates are shown in (d)–(f), respectively [publication III].

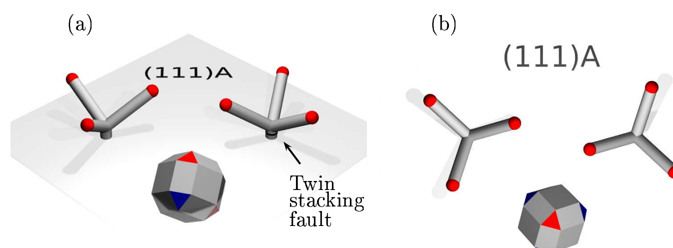

Figure 4.10: (a) Tilted view and (b) plan-view illustration of the effect of twinning during initial nanowire growth in [111]A direction on the number of azimuthal ⟨111⟩B growth directions [publication III].

strates have more weight at smaller diameters. The differences in nanowire lengths are more pronounced. Whereas the length distribution on (111)B substrate is very narrow, it is not so on (111)A and (110) substrates. Especially, growth on (110) resulted in nanowire lengths ranging from a few tens to a few hundred nanometers. That is clearly due to the large diameter distribution, resulting in smaller diameter nanowires losing the droplet very early in the growth process. According to the areal density of these nanowires, the number of seed particles is much higher on (110) sub-

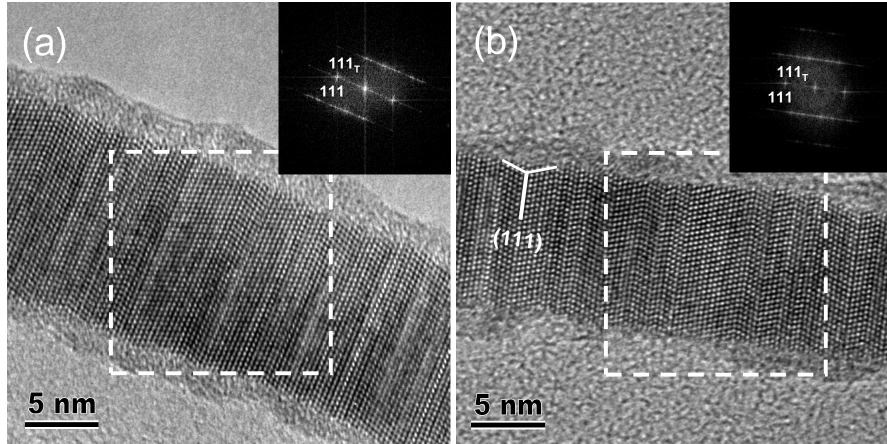

Figure 4.11: High-resolution TEM images of InP nanowires fabricated on (a) (111)A and (b) (110) substrate, respectively, with FFT insets calculated from the corresponding framed regions [publication III].

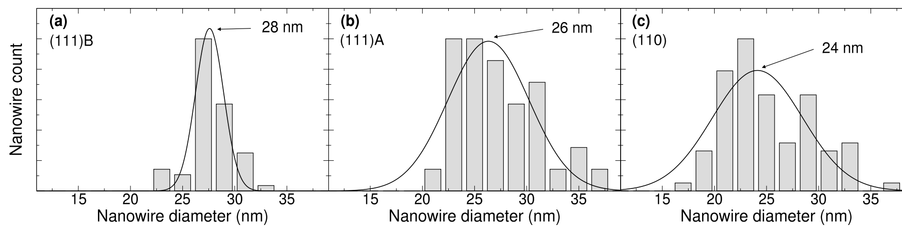

Figure 4.12: Diameter histograms for InP nanowires grown catalyst-free on (a) (111)B, (b) (111)A, and (c) (110) substrate. The curves are Gaussian fits to the data [publication III].

strates compared to other orientations. That could be due to an instability of the substrate surface during the droplet deposition step and formation of efficient sinks for indium through surface faceting. A number of nanowires are seeded by small, unstable droplets that are consumed or evaporated quickly at the beginning of the growth process, resulting in a high density of short and highly tapered nanowires.

On InP substrates InP nanowires tend to grow in the $\langle 111 \rangle$B directions in correlation with the substrate crystal structure. In the case of publication II, where nanowire growth was not epitaxial on silicon, different behavior was observed. TEM images of linear InP nanowire segments originally grown on silicon are shown in Fig. 4.13. The first thing to be noted in the low-magnification image in Fig. 4.13(a) is that there seem to be no twin stacking faults. This is explained by the high-resolution TEM image and electron diffraction pattern in Fig. 4.13(b) showing that the crystalline structure is wurtzite and that the c axis of the lattice is perpendicular to the nanowire axis. This has been reported for laser-assisted-catalytic-grown GaN nanowires [36] but not for InP. In some nanowires, there was also some evidence of twin planes parallel to the nanowire axis. Given the rotated growth direction, that

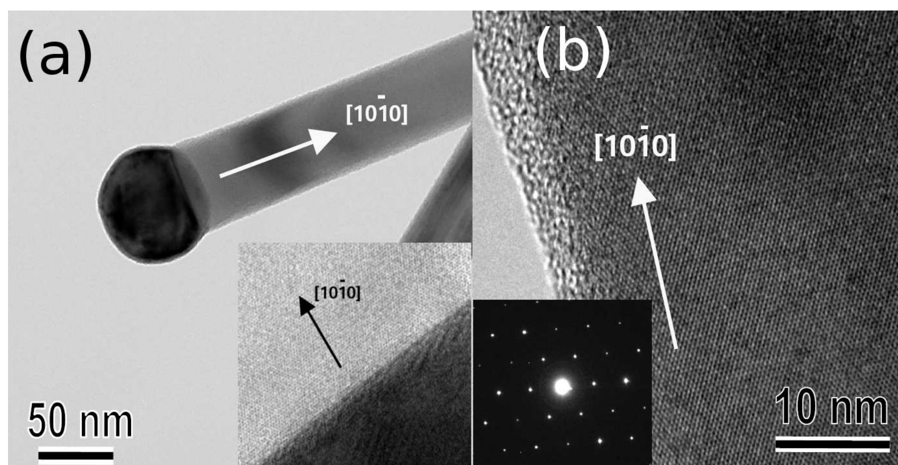

Figure 4.13: (a) TEM image of a catalyst-free-grown InP nanowire grown on Si (111). A close-up of the droplet-core interface is shown in the inset. (b) High-resolution TEM image of the same wire, and an electron diffraction pattern taken perpendicularly to the nanowire axis [publication II].

is not totally unexpected. Similar growth behavior has been reported for GaN [100] and SiGe [101] nanowires. As the edges of the twin planes always reside at the liquid–solid interface, they can act as efficient nucleation sites for InP precipitation. That would explain the higher growth rate observed in section 4.2 on silicon substrates. However, such twinning was not observed in every nanowire. Also, due to the different growth direction, nucleation at the liquid–solid interface can be more efficient and lead to higher growth rates. Then again, since the growth parameters for non-tapered nanowires are the same on silicon and InP substrates, the higher growth rate would mean better capture efficiency of constituents from the vapor phase. It remains unclear why that would be substrate dependent.

4.4 Nanowire photoluminescence

The photoluminescence of low-dimensional semiconductor structures is modified by quantum confinement. The Bohr exciton radius is considered the size limit for the thickness of a quantum well or the diameter of a quantum wire for confinement effects to occur. In indium phosphide it is about 15 nm [102]. Very often VLS grown nanowires are larger in diameter and no quantum confinement effects are expected. However, as soon as the size limit is reached the states of electrons and holes are moved up in energy and nanowires become quantum wires. This is seen as a blue shift in the photoluminescence spectrum. Quantum wires also show giant polarization anisotropy in the optical transitions as a result of an intrinsic property of the band-structure [103]. However, also larger nanowires exhibit polarization anisotropy attributed to the large dielectric constrast between the semiconductor material and

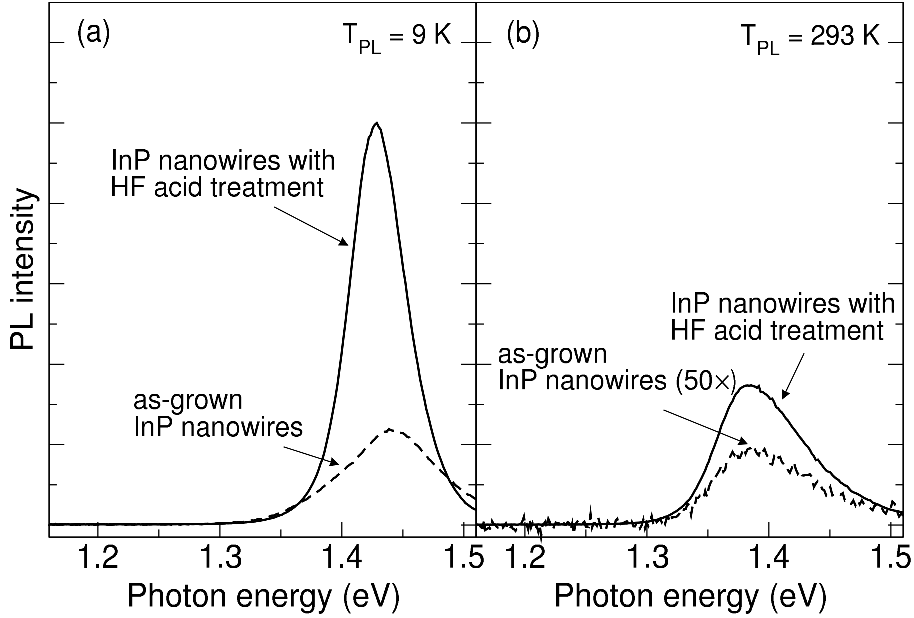

Figure 4.14: Photoluminescence spectra of as-grown and HF acid treated InP nanowires measured at (a) 9 K and (b) 293 K [publication IV].

the surrounding vacuum [83]. All catalyst-free-grown homoepitaxial InP nanowires in this work exhibited room-temperature photoluminescence. The maxima of ensemble PL spectra were all slightly blue shifted from the bulk zinc-blende InP band edge energy. This anomalous blue shift has been reported before for large-diameter InP nanowires, where no quantum confinement effects are expected [47, 102]. Based on PL measurements on nanowire ensembles with different size distributions, quantum confinement is not contributing here either. Single-nanowire PL measurements were not performed. The blue shift was speculated to stem from small effective nanowire diameter due to surface depletion [6], high density of twin stacking faults, or presence of wurtzite sections. Moreover, spectral shifts have been proposed to arise from Fermi level pinning in doped InP nanowires [104].

The sensitivity of the electrical and optical properties of nanowires can be used as an advantage in, *e.g.*, gas sensors, as discussed in section 2. However, in optically active low-dimensional devices an as-grown semiconductor surface acts as an efficient route for non-radiative carrier recombination, and the situation can be made even worse by elements adsorbed on the surface from the surrounding atmosphere. The passivation of catalyst-free-grown InP nanowire surfaces was demonstrated in publication IV by comparing the photoluminescence properties of as-grown nanowires and nanowires dipped into 50 % hydrofluoric (HF) acid for 1 minute before characterization. Silicon surface is known to be effectively passivated by hydrogen termination resulting from a HF acid treatment [105]. Similar passivating behavior has been predicted theoretically for hydrogen layers on InP nanowires [106]. Photoluminescence spectra measured from as-grown and HF acid treated InP nanowires are shown in Fig. 4.14.

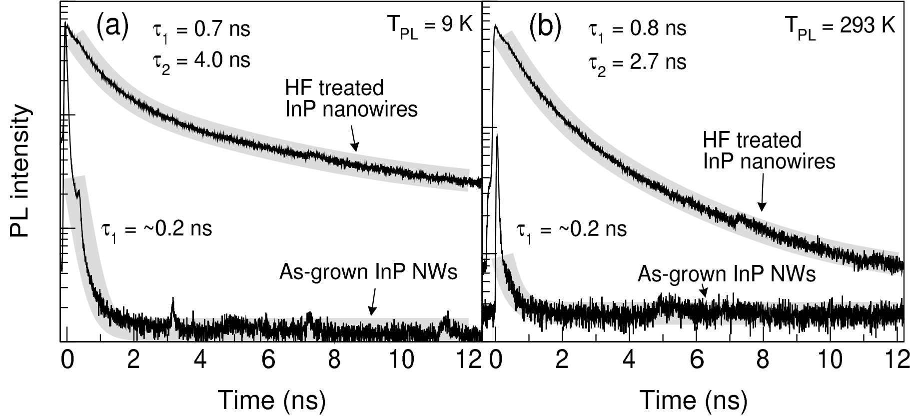

Figure 4.15: Time-resolved photoluminescence decay curves of as-grown and HF treated InP nanowires measured at (a) 9 K and (b) 293 K. Double-exponential fits are shown in light gray [publication IV].

A significant increase in the PL intensity after HF acid treatment can be observed at room temperature (90×). At 9 K the effect is about one order of magnitude smaller. Also in this case, a blue shift of about 20–30 meV in the PL peak energy compared to the band gap energy of zinc-blende InP (1.42 eV and 1.35 eV at 9 K and 293 K, respectively [107]) was observed, and it was not affected by the surface treatment or excitation intensity. The full width at half maximum (FWHM) of both PL peaks was about 100 meV at room tempearature. The HF acid treatment decreased the 9 K PL peak FWHM from 100 meV to about 60 meV. It must be noted that while measuring an ensemble instead of single nanowires, some broadening effects may be caused by the size distribution in the ensemble. However, the FWHM of about 100 meV is in line with previous single-nanowire results [102], where the broadening was attributed to surface states and fluctuations in single-nanowire diameter. The PL peak width could also depend on the excitation intensity.

TEM imaging was used to see effect of the HF treatment on the nanowire morphology (images not shown here). The indium droplet vanishes in the treatment, but there is no noticeable difference in the average nanowire diameter. High-resolution TEM images revealed an amorphous layer with a thickness of 1–2 nm, consisting mostly of carbon, on the surface of both treated and as-grown nanowires, which may have had been the result of electron beam induced damage. The passivation effect here is in line with previous reports of photoactivated InP nanocrystal passivation using HF containing solutions [108, 109]. In those studies, it was proposed that the effect would be due to fluorine. However, no traces of fluorine were observed in the EDS analyses performed on the HF treated nanowires in this work.

The photoluminescence dynamics were studied using time-resolved photoluminescence (TRPL) measurements. PL decay curves measured from HF treated and as-grown InP nanowires are shown in Fig. 4.15. The curves measured from HF

treated nanowires clearly are not single-exponential. A double-exponential function

$$f(t) = \Gamma_1 \exp(-t/\tau_1) + \Gamma_2 \exp(-t/\tau_2) + C \qquad (4.1)$$

was fitted to the experimental TRPL data by adjusting Γ_i, τ_i, and C. The decay times can be written as $\tau_i = \tau_{\mathrm{R},i}^{-1} + \tau_{\mathrm{NR},i}^{-1}$, where $\tau_{\mathrm{R},i}$ and $\tau_{\mathrm{NR},i}$ is the radiative and non-radiative carrier life time, respectively. The constant C takes care of the noise background. Only one decay time was extracted from the as-grown nanowire TRPL data due to insufficient signal-to-noise ratio. The fitting results are shown in Fig. 4.15. The two carrier life times of passivated nanowires are about 1 ns and 3–4 ns. Although reports of time-resolved photoluminescence measurements on III–V nanowires without core–shell structures are scarce, multi-exponential PL decay behavior has been reported from GaN [110] and large-diameter GaAs [6] nanowires. The behavior has been attributed to band bending effects caused by surface states and their screening at high carrier concentrations after high-intensity excitation pulses [111, 112]. The fast decay process is due to recombination via surface states in a flat-band condition. As the decay of as-grown nanowires is dominated by the fast process, the density of surface states in them is higher or the nature of the defects is different than in HF treated nanowires. Multi-exponential fluorescence decay has been shown in CdSe nanocrystals to result from fluorescence blinking effects [113] that are also seen in the photoluminescence dynamics of InP nanowires [109]. As it was pointed out earlier, one advantage of the catalyst-free VLS method over the conventional one is that the incorporation of third-party atoms, for example gold, is avoided. Although the solubility of gold in InP is rather low [114], gold doping might still affect the optical properties. Thus, as long as the surface recombination on nanowires is taken care of, time-resolved photoluminescence measurements could provide a means to quantify the effect of incorporated gold atoms on the carrier life times.

In(As)P nanowires grown on silicon in publication II were characterized by room temperature PL measurements. The spectra are plotted in Fig. 4.16. First, the PL of pure InP nanowires in Fig. 4.16 exhibit no blue shift in contrast to PL from catalyst-free-grown homoepitaxial InP nanowires. Considering the hexagonal crystal structure of the nanowires, this result is somewhat in contradiction with studies of wurtzite InP nanowire photoluminescence [Ref. 47 and publication V]. However, the lack of blue shift may be due to the different crystalline orientation of the nanowires – the c axis being perpendicular to the nanowire axis – which has been shown to affect the PL properties of hexagonal GaN nanowires through surface effects [115] or GaN quantum wells through piezoelectric effects [116]. In nanowires, further modifications result from possible quantum confinement and strain [117].

PL measured from InAsP nanowires in Fig. 4.16 exhibited two intensity peaks, one at the energy of pure InP nanowires and another at slightly lower energies. As a clear correlation between the position of the lower energy peak and the TBA molar

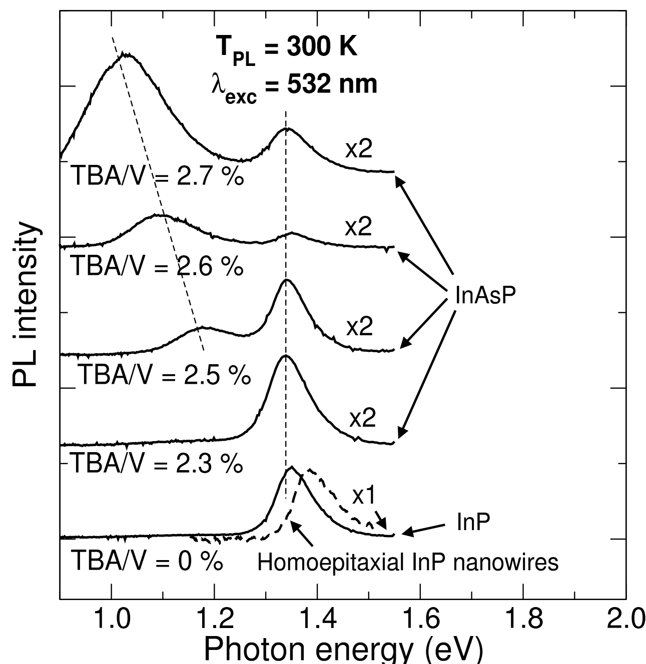

Figure 4.16: Room-temperature photoluminescence spectra from In(As)P nanowires grown on (111) Si with various TBA/V molar ratios. The vertical offsets between the spectra have been added for clarity. The dashed curve shows a spectrum measured from catalyst-free-grown homoepitaxial InP nanowires [publication II].

ratio during nanowire growth was observed, it was proposed that the peak was due to photoluminescence from $InAs_{1-x}P_x$. EDS analyses of the nanowires revealed that the nanowires were mostly pure InP with segments of InAsP, which explains the bimodal spectra. During growth both TBP and TBA were flowing into the reactor at a constant rate. Thus, the inhomogeneous distribution of arsenic is surprising. However, the growth of such segmented wires can be understood by comparing the solubilities of arsenic and phosphorus into liquid indium. The equilibrium arsenic concentration in liquid indium at 350 °C is about 1 atom-%, about ten times that of phosphorus [8]. At low arsenic partial pressures in the reactor and since there is no arsenic in the substrate, the supersaturation condition for arsenic is fulfilled at a later time compared to phosphorus. Thus, at least at the beginning of nanowire growth, only InP is precipitated. Finally, as arsenic concentration reaches supersaturation, InAsP is precipitated. The segmentation might be due to different diffusion velocities of arsenic and phosphorus in liquid indium. Here, however, the In–P and In–As systems are considered separate and the effects of the co-existence of phosphorus and arsenic in the liquid are neglected.

5 Gold-nanoparticle-catalyzed indium phosphide nanowires

5.1 Nanowire growth

InP nanowire growth using the conventional method with gold nanoparticle catalysts was studied in publication V. Gold nanoparticles were dispersed on (111)B InP substrates from a colloidal solution consisting of particles nominally 20 nm in diameter. To enhance nanoparticle adhesion, the substrates were treated with poly-l-lysine prior to nanoparticle deposition. A similar growth sequence to catalyst-free InP nanowire growth was used here. In contrast to catalyst-free growth, however, the growth temperatures were about 100 °C higher. That is slightly lower than the eutectic formation for the bulk Au–In system [8]. However, it has been shown that already these particle sizes can lead to melting point depression [118]. SEM images from samples grown at temperatures between 420 °C and 450 °C are shown in Fig. 5.1. In this particular series, 430 °C was the optimal temperature for uniform-diameter nanowires. Higher temperatures resulted in nanowire tapering and plateau formation at the base. The vertical growth orientation was lost at lower growth temperature. Growth at 430 °C resulted in an average nanowire length of about 2.5 µm (growth rate about 24 nm/s), an areal density of about $7 \cdot 10^8$ cm^{-2} and a diameter of about 50 nm.

Compared to InP nanowires fabricated using the catalyst-free method, one distinct difference can be observed. The average growth rate was about 24 nm/s, approximately ten times the growth rate of catalyst-free homoepitaxial InP nanowires at 350 °C and about the same as the catalyst-free growth rate observed on silicon. A major contributor to the increased growth rate is the higher decomposition probability of TBP at higher growth temperatures. Moreover, the droplet material (indium or gold) probably affects the adsorption efficiency of TBP or phosphorus, and may chemically catalyze the decomposition of TBP.

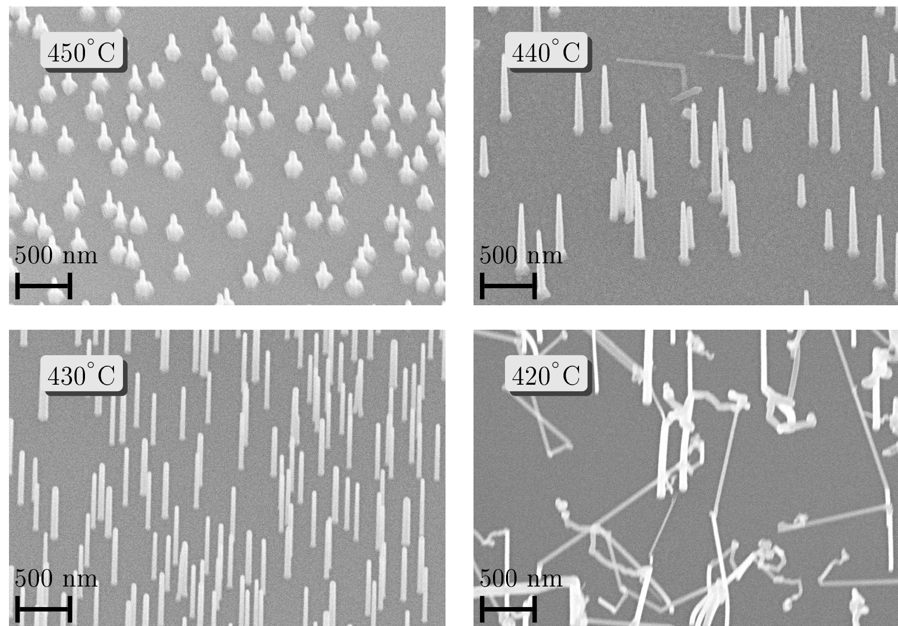

Figure 5.1: SEM images of gold-nanoparticle-catalyzed InP nanowire samples grown at four different temperatures [publication V].

5.2 Photoluminescence and crystal structure

The room temperature PL spectra measured from the gold-nanoparticle-catalyzed InP nanowires are shown in Fig. 5.2(a). The PL intensity of nanowires grown at 420 °C peaks at 1.35 eV, the band gap energy of bulk zinc-blende InP, whereas the spectra measured from nanowires grown at higher temperatures exhibited a blue shift of about 80 meV. Here, too, the nanowire diameter is large enough (∼50 nm) to rule out blue shift due to quantum confinement. X-ray diffraction maps measured around the 111 reflection of zinc-blende InP are shown in Fig. 5.2(b)–(d). The samples with vertical nanowires that exhibited blue shifted PL also showed an extra diffraction peak at approximately 0.05° smaller $\omega/2\theta$ angle than the zinc-blende (111) peak. This peak was not observed in diffraction maps measured from reference samples without nanowires. Moreover, it was not observed in a diffraction map measured from the sample grown at 420 °C not exhibiting blue shifted PL. However, this diffraction peak can be lost due to the random orientation of the nanowires grown at 420 °C. Nevertheless, in publication V the small-angle peak was proposed to arise from (0002) diffraction of wurtzite InP, thus, indicating that the nanowires had crystallized, at least partially, in a hexagonal crystal structure. The observed blue shift in the PL spectra were found to be in good agreement with theoretical predictions for the bang-gap energy of wurtzite InP [119].

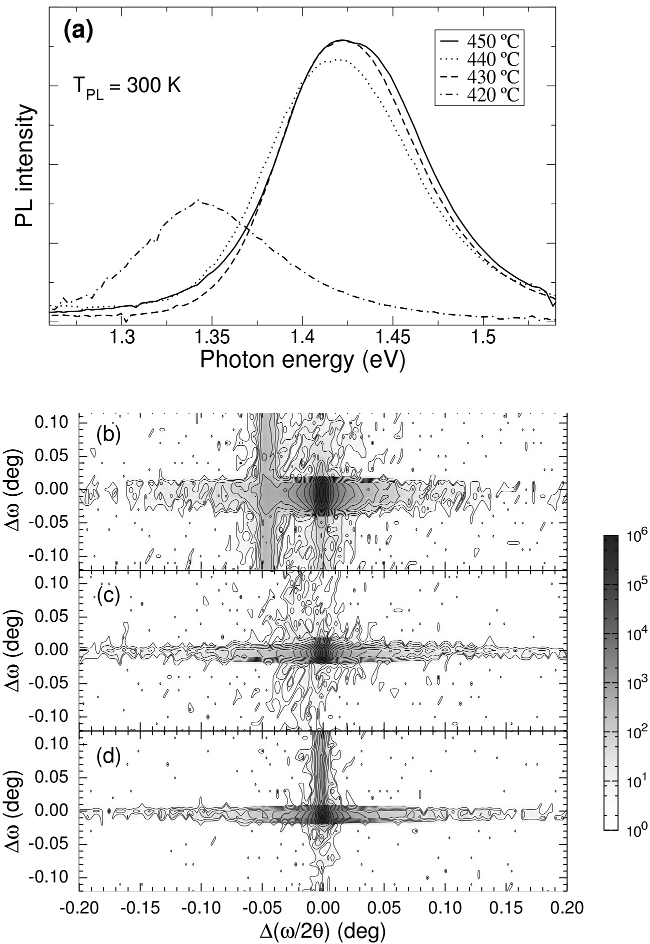

Figure 5.2: (a) Room temperature PL spectra measured from gold-nanoparticle-catalyzed InP nanowires grown at 420–450 °C. Two-axis XRD maps around InP 111 reflection from InP nanowire samples grown at (b) 440 °C, (c) 420 °C, and (d) (111)B InP substrate [publication V].

6 Summary and outlook

In the work presented in this thesis, the fabrication of InP nanowires using metalorganic vapor phase epitaxy was studied. The nanowires were formed by self-assembled growth utilizing the vapor-liquid-solid method. Typically III–V compound semiconductor nanowires are fabricated using gold nanoparticle catalyzed VLS growth. The studies presented here concentrated mainly on a new catalyst-free method using *in situ* deposited indium droplets as seeds for nanowire growth.

Homoepitaxial catalyst-free-grown InP nanowires were successfully fabricated on variously oriented substrates with typical diameters of around 20–30 nm, lengths of a few hundred nanometers, and areal densities of about 10^9 cm^{-2}. Growth-time tailoring of nanowire dimensions was demonstrated using the *in situ* technique. Electron microscopy characterization of individual nanowires revealed mostly zinc-blende crystal structure with twin stacking faults, both typical for vapor-liquid-solid-grown nanowires. Growth on silicon substrate was non-epitaxial, resulting in a hexagonal crystalline structure and an unconventional growth direction with the c axis perpendicular to the nanowire axis.

With optoelectronic applications in mind, the fabricated nanowires were characterized optically using photoluminescence spectroscopy. The nanowire samples were optically active at room temperature, exhibiting an anomalous blue shift. A significant increase in the photoluminescence intensity was observed after a hydrofluoric acid treatment of the nanowires. The unorthodox crystalline structure of nanowires grown on silicon was reflected in the photoluminescence spectra as a missing blue shift.

Finally, growth of InP nanowires using the conventional gold nanoparticle catalyzed growth method was studied. A growth-parameter-dependent blue shift in the photoluminescence spectra was observed. Based on x-ray diffraction analysis it was proposed that the blue shift was caused by nanowire crystallization in the wurtzite structure.

The work presented in this thesis concentrated mainly on binary InP nanowires. For future work with the goal of advancing towards simple devices, the catalyst-free fabrication method should be extended to ternary compounds for wavelength tunability, and radial and axial heterostructures for quantum confinement effects,

such as resonance tunneling in carrier transport. For electrical operation, n and p type doping of catalyst-free grown nanowires should be explored. The simplest way to produce p-n junctions would be to grow n type nanowires on a p type substrate or vice versa. Different dopant solubilities in the liquid phase may place some restrictions on the abruptness of p-n junctions and heterointerfaces in catalyst-free fabrication. Nevertheless, the optical properties and dimensions demonstrated in this work are suitable for device fabrication. The first device based on catalyst-free nanowires has yet to be demonstrated.

References

[1] R. S. Wagner and W. C. Ellis, Appl. Phys. Lett. **4**, 89 (1964).

[2] M. Law, J. Goldberger and P. Yang, Annu. Rev. Mater. Res. **34**, 83 (2004).

[3] W. Lu and C. M. Lieber, J. Phys. D: Appl. Phys. **39**, R387 (2006).

[4] Y. Xia, P. Yang, Y. Sun, Y. Wu, B. Mayers, B. Gates, Y. Yin, F. Kim and H. Yan, Adv. Mater. **15**, 353 (2003).

[5] A. P. Levitt, ed., *Whisker Technology* (John Wiley & Sons, Inc., USA, 1970), chap. 3, p. 47–119.

[6] K. Hiruma, M. Yazawa, T. Katsuyama, K. Ogawa, K. Haraguchi, M. Koguchi and H. Kakibayashi, J. Appl. Phys. **77**, 447 (1995).

[7] S. Bhunia, T. Kawamura, Y. Watanabe, S. Fujikawa and K. Tokushima, Appl. Phys. Lett. **83**, 3371 (2003).

[8] T. B. Massalski, ed., *Binary Alloy Phase Diagrams* (American Society for Metals, USA, 1986), vol. 2, p. 205, 260, 268, 1388.

[9] J. Zhang and L. Zhang, J. Vac. Sci. Technol. B **21**, 2415 (2003).

[10] E. I. Givargizov, J. Cryst. Growth **31**, 20 (1975).

[11] J. Johansson, B. A. Wacaser, K. A. Dick and W. Seifert, Nanotechnology **17**, S355 (2006).

[12] M. A. Verheijen, G. Immink, T. de Smet, M. T. Borgström and E. P. A. M. Bakkers, J. Am. Chem. Soc. **128**, 1353 (2006).

[13] G. A. Bootsma and H. J. Gassen, J. Cryst. Growth. **10**, 223 (1971).

[14] E. Ertekin, P. A. Greaney, D. C. Chrzan and T. D. Sands, J. Appl. Phys. **97**, 114325 (2005).

[15] T. Mårtensson, C. P. T. Svensson, B. A. Wacaser, M. W. Larsson, W. Seifert, K. Deppert, A. Gustafsson, L. R. Wallenberg and L. Samuelson, Nano Lett. **4**, 1987 (2004).

[16] S.-G. Ihn, J.-I. Song, T.-W. Kim, D.-S. Leem, T. Lee, S.-G. Lee, E. K. Koh and K. Song, Nano Lett. **7**, 39 (2007).

[17] E. P. A. M. Bakkers, J. A. van Dam, S. de Franceschi, L. P. Kouwenhoven, M. Kaiser, M. Verheijen, H. Wondergem and P. van der Sluis, Nature Mater. **3**, 769 (2004).

[18] L. J. Lauhon, M. S. Gudiksen and C. M. Lieber, Phil. Trans. R. Soc. Lond. A **362**, 1247 (2004).

[19] K. Hiruma, H. Murakoshi, M. Yazawa and T. Katsuyama, J. Cryst. Growth **163**, 226 (1996).

[20] M. T. Björk, B. J. Ohlsson, T. Sass, A. I. Persson, C. Thelander, M. H. Magnusson, K. Deppert, L. R. Wallenberg and L. Samuelson, Nano Lett. **2**, 87 (2002).

[21] Z. Zanolli, L. E. Fröberg, M. T. Björk, M.-E. Pistol and L. Samuelson, Thin Solid Films **515**, 793 (2006).

[22] N. Sköld, L. S. Karlsson, M. W. Larsson, M.-E. Pistol, W. Seifert, J. Trägårdh and L. Samuelson, Nano Lett. **5**, 1943 (2005).

[23] M. T. Borgström, M. A. Verheijen, G. Immink, T. de Smet and E. P. A. M. Bakkers, Nanotechnology **17**, 4010 (2006).

[24] C. P. T. Svensson, W. Seifert, M. W. Larsson, L. R. Wallenberg, J. Stangl, G. Bauer and L. Samuelson, Nanotechnology **16**, 936 (2005).

[25] J. P. Spatz, S. Mössmer, C. Hartmann, M. Möller, T. Herzog, M. Krieger, H.-G. Boyen, P. Ziemann and B. Kabius, Langmuir **16**, 407 (2000).

[26] M. Haupt, S. Miller, R. Glass, M. Arnold, R. Sauer, K. Thonke, M. Möller and J. P. Spatz, Adv. Mater. **15**, 829 (2003).

[27] Z. H. Wu, X. Y. Mei, D. Kim, M. Blumin and H. E. Ruda, Appl. Phys. Lett. **81**, 5177 (2002).

[28] B. J. Ohlsson, M. T. Björk, M. H. Magnusson, K. Deppert, L. Samuelson and L. R. Wallenberg, Appl. Phys. Lett. **79**, 3335 (2001).

[29] W. Seifert, M. Borgström, K. Deppert, K. A. Dick, J. Johansson, M. W. Larsson, T. Mårtensson, N. Sköld, C. P. T. Svensson, B. A. Wacaser, L. R. Wallenberg and L. Samuelson, J. Cryst. Growth **272**, 211 (2004).

[30] X. Wang, C. J. Summers and Z. L. Wang, Nano Lett. **4**, 423 (2004).

[31] D. F. Liu, Y. J. Xiang, X. C. Wu, Z. X. Zhang, L. F. Liu, L. Song, X. W. Zhao, S. D. Luo, W. J. Ma, J. Shen, W. Y. Zhou, G. Wang, C. Y. Wang and S. S. Xie, Nano Lett. **6**, 2375 (2006).

[32] T. Mårtensson, M. Borgström, W. Seifert, B. J. Ohlsson and L. Samuelson, Nanotechnology **14**, 1255 (2003).

[33] T. Mårtensson, P. Carlberg, M. Borgström, L. Montelius, W. Seifert and L. Samuelson, Nano Lett. **4**, 699 (2004).

[34] A. M. Morales and C. M. Lieber, Science **279**, 208 (1998).

[35] X. Duan, J. Wang and C. M. Lieber, Appl. Phys. Lett. **76**, 1116 (2000).

[36] X. Duan and C. M. Lieber, J. Am. Chem. Soc. **122**, 188 (2000).

[37] Y. Wu, Y. Cui, L. Huynh, C. J. Barrelet, D. C. Bell and C. M. Lieber, Nano Lett. **4**, 433 (2004).

[38] V. Schmidt, S. Senz and U. Gösele, Nano Lett. **5**, 931 (2005).

[39] W. Braun, V. M. Kaganer, A. Trampert, H.-P. Schönherr, Q. Gong, R. Nötzel, L. Däweritz and K. H. Ploog, J. Cryst. Growth **227–228**, 51 (2001).

[40] N. Chetty and R. M. Martin, Phys. Rev. B **45**, 6089 (1992).

[41] S. Bhunia, T. Kawamura, S. Fujikawa, H. Nakashima, K. Furukawa, K. Torimitsu and Y. Watanabe, Thin Solid Films **464–465**, 244 (2004).

[42] Z. Ikonić, G. P. Srivastava and J. C. Inkson, Phys. Rev. B **48**, 17181 (1993).

[43] J. Johansson, L. S. Karlsson, C. P. T. Svensson, T. Mårtensson, B. A. Wacaser, K. Deppert, L. Samuelson and W. Seifert, Nature Mater. **5**, 574 (2006).

[44] M. Koguchi, H. Kakibayashi, M. Yazawa, K. Hiruma and T. Katsuyama, Jpn. J. Appl. Phys. **31**, 2061 (1992).

[45] S. Bhunia, T. Kawamura, S. Fujikawa, K. Tokushima and Y. Watanabe, Physica E **21**, 583 (2004).

[46] T. Akiyama, K. Nakamura and T. Ito, Phys. Rev. B **73**, 235308 (2006).

[47] P. Mohan, J. Motohisa and T. Fukui, Nanotechnology **16**, 2903 (2005).

[48] Z. Z. Bandić, T. C. McGill and Z. Ikonić, Phys. Rev. B **56**, 3564 (1997).

[49] Q. Xiong, J. Wang and P. C. Eklund, Nano Lett. **6**, 2736 (2006).

[50] A. Piotrowska, P. Auvray, A. Guivarc'h, G. Pelous and P. Henoc, J. Appl. Phys. **52**, 5112 (1981).

[51] A. Wohlfart, A. Devi, E. Maile and R. A. Fischer, Chem. Commun. p. 998–999 (2002).

[52] H. Parala, A. Devi, F. Hipler, E. Maile, A. Birkner, H. W. Becker and R. A. Fischer, J. Cryst. Growth **231**, 68 (2001).

[53] S. Vaddiraju, A. Mohite, A. Chin, M. Meyyappan, G. Sumanasekera, B. W. Alphenaar and M. K. Sunkara, Nano Lett. **5**, 1625 (2005).

[54] C. J. Novotny and P. K. L. Yu, Appl. Phys. Lett. **87**, 203111 (2005).

[55] M. Wei, D. Zhi and J. L. MacManus-Driscoll, Nanotechnology **16**, 1364 (2005).

[56] E. A. Stach, P. J. Pauzauskie, T. Kuykendall, J. Goldberger, R. He and P. Yang, Nano Lett. **3**, 867 (2003).

[57] M. Gherasimova, J. Su, G. Cui, Z.-Y. Ren, S.-R. Jeon, J. Han, Y. He, Y.-K. Song, A. V. Nurmikko, D. Ciuparu and L. Pfefferle, phys. stat. sol. (c) **2**, 2361 (2005).

[58] L. Hong, Z. Liu, X. T. Zhang and S. K. Hark, Appl. Phys. Lett. **89**, 193105 (2006).

[59] S. Noor Mohammad, J. Chem. Phys. **125**, 094705 (2006).

[60] H. Lipsanen, M. Sopanen and J. Ahopelto, Phys. Rev. B **51**, 13868 (1995).

[61] P. J. Poole, J. Lefebvre and J. Fraser, Appl. Phys. Lett. **83**, 2055 (2003).

[62] J. Noborisaka, J. Motohisa and T. Fukui, Appl. Phys. Lett. **86**, 213102 (2005).

[63] H. Z. Zhang, Y. C. Kong, Y. Z. Wang, X. Du, Z. G. Bai, J. J. Wang, D. P. Yu, Y. Ding, Q. L. Hang and S. Q. Feng, Solid State Commun. **109**, 677 (1999).

[64] Z. R. Dai, Z. W. Pan and Z. L. Wang, Adv. Funct. Mater. **13**, 9 (2003).

[65] K. A. Dick, K. Deppert, T. Mårtensson, B. Mandl, L. Samuelson and W. Seifert, Nano Lett. **5**, 761 (2005).

[66] R.-Q. Zhang, Y. Lifshitz and S.-T. Lee, Adv. Mater. **15**, 635 (2003).

[67] L. E. Greene, M. Law, J. Goldberger, F. Kim, J. C. Johnson, Y. Zhang, R. J. Saykally and P. Yang, Angew. Chem. Int. Ed. **42**, 3031 (2003).

[68] K. Haraguchi, T. Katsuyama, K. Hiruma and K. Ogawa, Appl. Phys. Lett. **60**, 745 (1992).

[69] Y. Huang, X. Duan, Y. Cui and C. M. Lieber, Nano Lett. **2**, 101 (2002).

[70] X. Duan, Y. Huang, Y. Cui, J. Wang and C. M. Lieber, Nature **409**, 66 (2001).

[71] M. T. Björk, B. J. Ohlsson, C. Thelander, A. I. Persson, K. Deppert, L. R. Wallenberg and L. Samuelson, Appl. Phys. Lett. **81**, 4458 (2002).

[72] X. Duan, Y. Huang, R. Agarwal and C. M. Lieber, Nature **421**, 241 (2003).

[73] A. B. Greytak, C. J. Barrelet, Y. Li and C. M. Lieber, Appl. Phys. Lett. **87**, 151103 (2005).

[74] C. Thelander, H. A. Nilsson, L. E. Jensen and L. Samuelson, Nano Lett. **5**, 635 (2005).

[75] T. Bryllert, L.-E. Wernersson, T. Löwgren and L. Samuelson, Nanotechnology **17**, S227 (2006).

[76] P. M. Parthangal, R. E. Cavicchi and M. R. Zachariah, Nanotechnology **17**, 3786 (2006).

[77] J. C. Johnson, H.-J. Choi, K. P. Knutsen, R. D. Schaller, P. Yang and R. J. Saykally, Nature Mater. **1**, 106 (2002).

[78] M. H. Huang, S. Mao, H. Feick, H. Yan, Y. Wu, H. Kind, E. Weber, R. Russo and P. Yang, Science **292**, 1897 (2001).

[79] Q. Wan, Q. H. Li, Y. J. Chen, T. H. Wang, X. L. He, J. P. Li and C. L. Lin, Appl. Phys. Lett. **84**, 3654 (2004).

[80] K. M. Ip, Z. Liu, C. M. Ng and S. K. Hark, Nanotechnology **16**, 1144 (2005).

[81] J. Hahm and C. M. Lieber, Nano Lett. **4**, 51 (2004).

[82] T. I. Kamins, S. Sharma, A. A. Yasseri, Z. Li and J. Straznicky, Nanotechnology **17**, S291 (2006).

[83] J. Wang, M. S. Gudiksen, X. Duan, Y. Cui and C. M. Lieber, Science **293**, 1455 (2001).

[84] Y. Huang, X. Duan, Q. Wei and C. M. Lieber, Science **291**, 630 (2001).

[85] D. Whang, S. Jin, Y. Wu and C. M. Lieber, Nano Lett. **3**, 1255 (2003).

[86] D. Whang, S. Jin and C. M. Lieber, Nano Lett. **3**, 951 (2003).

[87] Y. Huang, X. Duan, Y. Cui, L. J. Lauhon, K.-H. Kim and C. M. Lieber, Science **294**, 1313 (2001).

[88] S. Jin, D. Whang, M. C. McAlpine, R. S. Friedman, Y. Wu and C. M. Lieber, Nano Lett. **4**, 915 (2004).

[89] G. B. Stringfellow, *Organometallic Vapor-Phase Epitaxy: Theory and Practice* (Academic Press, Inc., Boston (MA), 1989), p. 158, 180.

[90] T. I. Kamins, X. Li, R. S. Williams and X. Liu, Nano Lett. **4**, 503 (2004).

[91] M. Borgström, K. Deppert, L. Samuelson and W. Seifert, J. Cryst. Growth **260**, 18 (2004).

[92] Y. Wu and P. Yang, J. Am. Chem. Soc. **123**, 3165 (2001).

[93] V. G. Dubrovskii, N. V. Sibirev, G. E. Cirlin, J. C. Harmand and V. M. Ustinov, Phys. Rev. E **73**, 021603 (2006).

[94] J. Johansson, C. P. T. Svensson, T. Mårtensson, L. Samuelson and W. Seifert, J. Phys. Chem. B **109**, 13567 (2005).

[95] J. C. Harmand, G. Patriarche, N. Péré-Lapeme, M.-N. Mérat-Combes, L. Travers and F. Glas, Appl. Phys. Lett. **87**, 203101 (2005).

[96] S. M. Prokes and S. Arnold, Appl. Phys. Lett. **86**, 193105 (2005).

[97] A. L. Roest, M. A. Verheijen, O. Wunnicke, S. Serafin, H. Wondergem and E. P. A. M. Bakkers, Nanotechnology **17**, S271 (2006).

[98] Z. H. Wu, X. Mei, D. Kim, M. Blumin, H. E. Ruda, J. Q. Liu and K. L. Kavanagh, Appl. Phys. Lett. **83**, 3368 (2003).

[99] U. Krishnamachari, M. Borgstrom, B. J. Ohlsson, N. Panev, L. Samuelson, W. Seifert, M. W. Larsson and L. R. Wallenberg, Appl. Phys. Lett. **85**, 2077 (2004).

[100] D. Tham, C.-Y. Nam and J. E. Fischer, Adv. Funct. Mater. **16**, 1197 (2006).

[101] K.-K. Lew, L. Pan, E. C. Dickey and J. M. Redwing, Adv. Mater. **15**, 2073 (2003).

[102] M. S. Gudiksen, J. Wang and C. M. Lieber, J. Phys. Chem. B **106**, 4036 (2002).

[103] M. P. Persson and H. Q. Xu, Phys. Rev. B **70**, 161310 (2004).

[104] M. H. M. van Weert, O. Wunnicke, A. L. Roest, T. J. Eijkemans, A. Y. Silov, J. E. M. Haverkort, G. W. 't Hooft and E. P. A. M. Bakkers, Appl. Phys. Lett. **88**, 043109 (2006).

[105] G. W. Trucks, K. Raghavachari, G. S. Higashi and Y. J. Chabal, Phys. Rev. Lett. **65**, 504 (1990).

[106] T. M. Schmidt, Appl. Phys. Lett. **89**, 123117 (2006).

[107] I. Vurgaftman, J. R. Meyer and L. R. Ram-Mohan, J. Appl. Phys. **89**, 5815 (2001).

[108] D. V. Talapin, N. Gaponik, H. Borchert, A. L. Rogach, M. Haase and H. Weller, J. Phys. Chem. B **106**, 12659 (2002).

[109] L. K. van Vugt, S. J. Veen, E. P. A. M. Bakkers, A. L. Roest and D. Vanmaekelbergh, J. Am. Chem. Soc. **127**, 12357 (2005).

[110] J. Yoo, Y.-J. Hong, S. J. An, G.-C. Yi, B. Chon, T. Joo, J.-W. Kim and J.-S. Lee, Appl. Phys. Lett. **89**, 043124 (2006).

[111] E. Yablonovitch, C. J. Sandroff, R. Bhat and T. Gmitter, Appl. Phys. Lett. **51**, 439 (1987).

[112] E. Yablonovitch, B. J. Skromme, R. Bhat, J. P. Harbison and T. J. Gmitter, Appl. Phys. Lett. **54**, 555 (1989).

[113] G. Schlegel, J. Bohnenberger, I. Potapova and A. Mews, Phys. Rev. Lett. **88**, 137401 (2002).

[114] V. Parguel, P. N. Favennec, M. Gauneau, Y. Rihet, R. Chaplain, H. L'Haridon and C. Vaudry, J. Appl. Phys. **62**, 824 (1987).

[115] A. H. Chin, T. S. Ahn, H. Li, S. Vaddiraju, C. J. Bardeen, C.-Z. Ning and M. K. Sunkara, Nano Lett. **7**, 626 (2007).

[116] P. Waltereit, O. Brandt, A. Trampert, H. T. Grahn, J. Menniger, M. Ramsteiner, M. Reiche and K. H. Ploog, Nature **406**, 865 (2000).

[117] T. Kuykendall, P. J. Pauzauskie, Y. Zhang, J. Goldberger, D. Sirbuly, J. Denlinger and P. Yang, Nature Mater. **3**, 524 (2004).

[118] H. D. Park, A.-C. Gaillot, S. M. Prokes and R. C. Cammarata, J. Cryst. Growth **296**, 159 (2006).

[119] M. Murayama and T. Nakayama, Phys. Rev. B **49**, 4710 (1994).

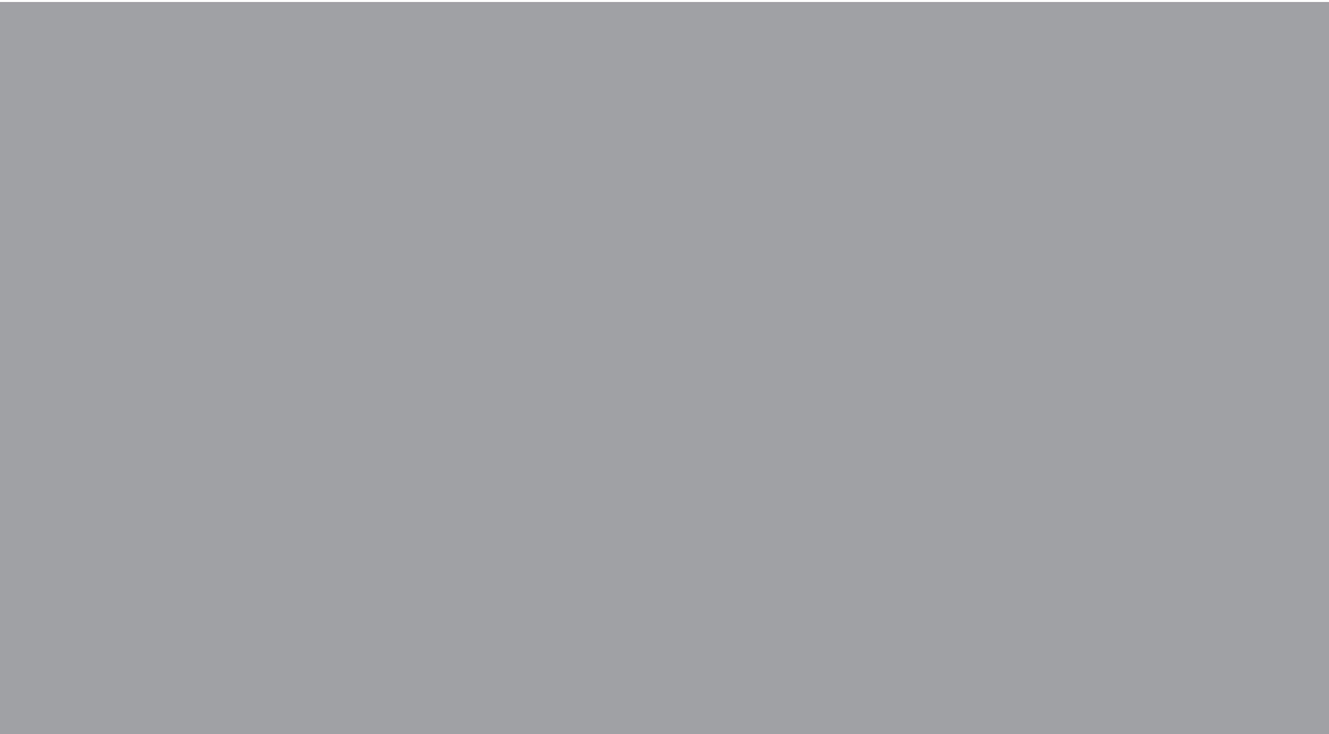

ISBN 978-951-22-8812-0
ISBN 978-951-22-8813-7 (PDF)
ISSN 1795-2239
ISSN 1795-4584 (PDF)